fail to establish two barriers that protect against dietary iron overload: the hepcidin-dependent intestinal barrier against iron hyperabsorption, and the FBXL5-dependent intracellular barrier against an inappropriate increase in the LIP. The aforementioned other mutant mice retain the latter barrier, which minimizes an inappropriate increase in the LIP. Thus, hepatic FBXL5 deficiency gives rise to iron poisoning that is more severe than that that results from simple systemic iron overload due to dietary iron excess.

Hepatic iron overload is a pathophysiologic feature of nonalcoholic steatohepatitis (NASH), chronic liver disease associated with hepatitis C virus infection, and hepatocellular carcinoma (Sorrentino et al., 2009). Excess ferrous iron generates hydroxyl radicals that give rise to chronic inflammation, DNA damage, genetic instability, and tumorigenesis as a result of oxidative stress. Although iron accumulation itself may not initiate chronic liver disease, it has a detrimental effect on disease progression. We have now shown that liver-specific ablation of FBXL5 results in an increased hepatic iron content, systemic iron overload, and acute fatal liver failure in the presence of dietary iron overload. *Alb*-Cre/*Fbxl5*$^{F/F}$ mice develop steatosis and inflammation of the liver, reminiscent of human NASH, likely as a result of mitochondrial damage. Increased serum iron levels might worsen the liver damage in *Alb*-Cre/*Fbxl5*$^{F/F}$ mice. Thus, we speculate that a reduced level of FBXL5 expression in the human liver might give rise to a vicious cycle of liver damage and contribute to the progression of chronic inflammation and liver cancer.

EXPERIMENTAL PROCEDURES

Generation of *Fbxl5*$^{-/-}$ and *Fbxl5*$^{-/-}$*Irp2*$^{-/-}$ Mice

The targeting vector for *Fbxl5* was constructed by replacement of a 3.1 kb fragment of genomic DNA containing exons 4 and 5 of *Fbxl5* with IRES-*lacZ* and PGK-*neo*-poly(A)-loxP cassettes. A diphtheria toxin A (DT-A) cassette was ligated at the 3′ end of the targeting construct. Maintenance, transfection, and selection of mouse ESCs were performed as described previously (Nakayama et al., 1996). Mutant ESCs were microinjected into C57BL/6 blastocysts, and resulting chimeras were mated with C57BL/6 mice. Heterozygous offspring were intercrossed to produce homozygous mutant animals and their littermate controls. For assessment of their growth capability, preimplantation embryos were cultured as described previously (Nishiyama et al., 2009). All mice in this study were backcrossed to the C57BL/6 background for more than six generations. *Fbxl5*$^{+/-}$ mice were also crossed with *Irp2*$^{-/-}$ mice (LaVaute et al., 2001) obtained from Mutant Mouse Regional Resource Centers. *Fbxl5*$^{+/-}$*Irp2*$^{+/-}$ offspring were intercrossed to produce *Fbxl5*$^{-/-}$*Irp2*$^{-/-}$ animals and their littermate controls.

Generation of Conditional Knockout Mice

The 5′ and 3′ regions of homology in the targeting vector for *Fbxl5* consisted of a 1.2 kb fragment of intron 3 and an 8.5 kb fragment spanning introns 3 and 7, respectively. The neomycin-resistance gene (*neo*) flanked by loxP sites was isolated from the plasmid pL2-Neo(2) (kindly provided by D.R. Littman) (Gu et al., 1993) and inserted upstream of exon 4 of *Fbxl5*. A loxP site was also inserted downstream of exon 5. ES clones that had undergone homologous recombination were transfected with pMC-Cre (kindly provided by D.R. Littman) to excise the loxP-*neo* cassette. Mutant ESCs were then microinjected into C57BL/6 blastocysts, and the resulting chimeras were mated with C57BL/6 mice. Heterozygous offspring were intercrossed to produce homozygous mutant animals (*Fbxl5*$^{F/F}$). *Fbxl5*$^{F/F}$ mice were then crossed with *Alb*-Cre transgenic mice (Postic and Magnuson, 2000) obtained from The Jackson Laboratory to produce *Alb*-Cre/*Fbxl5*$^{F/F}$ mice. A high-iron diet was formulated by supplementation of CA-1 (containing 0.03% [w/w] ferric citrate; CLEA Japan) with 2% (w/w) ferric citrate. All animals were maintained under the specific pathogen-free (SPF) condition, and all experiments were approved by the animal ethics committee of Kyushu University.

Iron Histochemistry

Mice (pregnant for analysis of embryos) were anesthetized by intravenous injection of pentobarbital sodium (648 mg/kg) and were then perfused consecutively with 50 mM hydrogen sulfide in deionized water and with 4% paraformaldehyde in phosphate-buffered saline. Iron was detected in cryostat sections by enhanced Perls or Turnbull staining. Tissue sections were washed with deionized water, incubated for 30 min with Perls reagent (5% potassium ferrocyanide, 5% HCl) or with Turnbull reagent (5% potassium ferricyanide, 5% HCl), and then washed again in deionized water before incubation first for 15 min with unactivated DAB (0.05% DAB in deionized water) and then for 10 min with activated DAB (0.05% DAB, 1% H_2O_2). Tissue sections of control and mutant mice were stained at the same time to allow monitoring and detection of nonspecific staining.

Whole-Mount In Situ Hybridization

Whole-mount in situ hybridization was performed as described previously (Nishiyama et al., 2009). An FBXL5 antisense riboprobe corresponding to nucleotides 396–765 of the cDNA was synthesized with the use of a DIG RNA labeling kit (Roche).

RT and Real-Time PCR Analysis

RT and real-time PCR analysis was performed as described previously (Onoyama et al., 2011). Purification of mRNA from embryos was performed with the use of a TurboCapture mRNA Kit (QIAGEN). The sequences of the PCR primers (forward and reverse, respectively) were: 5′-GGTGATCCATACA CACCTGGCTT-3′ and 5′-TGATGACTGAGATGGCGGAA-3′ for TfR1; 5′-CC TATCTCCATCAACAGAT-3′ and 5′-TGCAACAGATACCACACTG-3′ for hepcidin 1 (Hamp1); and 5′-GGACCCGAGAAGACCTCCTT-3′ and 5′-GCACATCAC TCAGAATTTCAATGG-3′ for ARBP (attachment region-binding protein). Reactions for ARBP mRNA were performed concurrently on the same plate as those for the test mRNAs, and results were normalized by the corresponding amount of ARBP mRNA.

Immunoblot Analysis

Immunoblot analysis was performed as previously described (Onoyama et al., 2011) with antibodies to IRP1 (sc-14216; Santa Cruz Biotechnology), to p150^{Glued} (610473; BD Transduction Laboratories), to phosphorylated Smad1(Ser$^{463/465}$)/Smad5(Ser$^{463/465}$)/Smad8(Ser$^{426/428}$) (9511; Cell Signaling Technology), to ferritin (F6136; Sigma-Aldrich), to TfR1 (13-6800; Invitrogen), to Hsp90 (610419; BD Biosciences), and to IRP2 (generated by K. Iwai, Osaka University).

Statistical Analysis

Quantitative data are presented as mean ± SEM or ± SD as indicated and were compared between groups with the two-tailed Student's t test as performed with Microsoft Excel software. A p value of <0.05 was considered statistically significant.

SUPPLEMENTAL INFORMATION

Supplemental Information includes Supplemental Experimental Procedures, Supplemental References, six figures, and two tables and can be found with this article online at doi:10.1016/j.cmet.2011.07.011.

ACKNOWLEDGMENTS

We thank T. Rouault for *Irp2*$^{-/-}$ mice; D.R. Littman for pL2-Neo(2) and pMC-Cre; T. Kitamura for pMX-puro; M. Tanaka, Y. Yamada, K. Takeda, M. Sasaki, R. Ugawa, M. Oda, E. Koba, and N. Kinoshita for technical assistance; and D. Kang, S. Toyokuni, S. Sakata, and T. Asano for discussion.

Received: March 30, 2011
Revised: June 23, 2011
Accepted: July 19, 2011
Published: September 6, 2011

REFERENCES

Andrews, N.C., and Schmidt, P.J. (2007). Iron homeostasis. Annu. Rev. Physiol. *69*, 69–85.

Burt, A.D. (2001). Steatosis and steatohepatitis. Curr. Diagn. Pathol. *7*, 141–147.

Cooperman, S.S., Meyron-Holtz, E.G., Olivierre-Wilson, H., Ghosh, M.C., McConnell, J.P., and Rouault, T.A. (2005). Microcytic anemia, erythropoietic protoporphyria, and neurodegeneration in mice with targeted deletion of iron-regulatory protein 2. Blood *106*, 1084–1091.

Cross, J.C., Werb, Z., and Fisher, S.J. (1994). Implantation and the placenta: key pieces of the development puzzle. Science *266*, 1508–1518.

De Domenico, I., McVey Ward, D., and Kaplan, J. (2008). Regulation of iron acquisition and storage: consequences for iron-linked disorders. Nat. Rev. Mol. Cell Biol. *9*, 72–81.

De Domenico, I., Vaughn, M.B., Li, L., Bagley, D., Musci, G., Ward, D.M., and Kaplan, J. (2006). Ferroportin-mediated mobilization of ferritin iron precedes ferritin degradation by the proteasome. EMBO J. *25*, 5396–5404.

Donovan, A., Lima, C.A., Pinkus, J.L., Pinkus, G.S., Zon, L.I., Robine, S., and Andrews, N.C. (2005). The iron exporter ferroportin/Slc40a1 is essential for iron homeostasis. Cell Metab. *1*, 191–200.

Galy, B., Ferring, D., Minana, B., Bell, O., Janser, H.G., Muckenthaler, M., Schümann, K., and Hentze, M.W. (2005). Altered body iron distribution and microcytosis in mice deficient in iron regulatory protein 2 (IRP2). Blood *106*, 2580–2589.

Gu, H., Zou, Y.R., and Rajewsky, K. (1993). Independent control of immunoglobulin switch recombination at individual switch regions evidenced through Cre-loxP-mediated gene targeting. Cell *73*, 1155–1164.

Hentze, M.W., Muckenthaler, M.U., Galy, B., and Camaschella, C. (2010). Two to tango: regulation of Mammalian iron metabolism. Cell *142*, 24–38.

Jin, J., Cardozo, T., Lovering, R.C., Elledge, S.J., Pagano, M., and Harper, J.W. (2004). Systematic analysis and nomenclature of mammalian F-box proteins. Genes Dev. *18*, 2573–2580.

Kautz, L., Meynard, D., Monnier, A., Darnaud, V., Bouvet, R., Wang, R.H., Deng, C., Vaulont, S., Mosser, J., Coppin, H., and Roth, M.P. (2008). Iron regulates phosphorylation of Smad1/5/8 and gene expression of Bmp6, Smad7, Id1, and Atoh8 in the mouse liver. Blood *112*, 1503–1509.

LaVaute, T., Smith, S., Cooperman, S., Iwai, K., Land, W., Meyron-Holtz, E., Drake, S.K., Miller, G., Abu-Asab, M., Tsokos, M., et al. (2001). Targeted deletion of the gene encoding iron regulatory protein-2 causes misregulation of iron metabolism and neurodegenerative disease in mice. Nat. Genet. *27*, 209–214.

Lesbordes-Brion, J.C., Viatte, L., Bennoun, M., Lou, D.Q., Ramey, G., Houbron, C., Hamard, G., Kahn, A., and Vaulont, S. (2006). Targeted disruption of the hepcidin 1 gene results in severe hemochromatosis. Blood *108*, 1402–1405.

MacKenzie, E.L., Iwasaki, K., and Tsuji, Y. (2008). Intracellular iron transport and storage: from molecular mechanisms to health implications. Antioxid. Redox Signal. *10*, 997–1030.

Meguro, R., Asano, Y., Iwatsuki, H., and Shoumura, K. (2003). Perfusion-Perls and -Turnbull methods supplemented by DAB intensification for nonheme iron histochemistry: demonstration of the superior sensitivity of the methods in the liver, spleen, and stomach of the rat. Histochem. Cell Biol. *120*, 73–82.

Meyron-Holtz, E.G., Ghosh, M.C., and Rouault, T.A. (2004a). Mammalian tissue oxygen levels modulate iron-regulatory protein activities in vivo. Science *306*, 2087–2090.

Meyron-Holtz, E.G., Ghosh, M.C., Iwai, K., LaVaute, T., Brazzolotto, X., Berger, U.V., Land, W., Ollivierre-Wilson, H., Grinberg, A., Love, P., and Rouault, T.A. (2004b). Genetic ablations of iron regulatory proteins 1 and 2 reveal why iron regulatory protein 2 dominates iron homeostasis. EMBO J. *23*, 386–395.

Muckenthaler, M.U., Galy, B., and Hentze, M.W. (2008). Systemic iron homeostasis and the iron-responsive element/iron-regulatory protein (IRE/IRP) regulatory network. Annu. Rev. Nutr. *28*, 197–213.

Nakayama, K., Ishida, N., Shirane, M., Inomata, A., Inoue, T., Shishido, N., Horii, I., Loh, D.Y., and Nakayama, K.I. (1996). Mice lacking p27(^{Kip1}) display increased body size, multiple organ hyperplasia, retinal dysplasia, and pituitary tumors. Cell *85*, 707–720.

Nakayama, K.I., and Nakayama, K. (2006). Ubiquitin ligases: cell-cycle control and cancer. Nat. Rev. Cancer *6*, 369–381.

Nemeth, E., Tuttle, M.S., Powelson, J., Vaughn, M.B., Donovan, A., Ward, D.M., Ganz, T., and Kaplan, J. (2004). Hepcidin regulates cellular iron efflux by binding to ferroportin and inducing its internalization. Science *306*, 2090–2093.

Niederkofler, V., Salie, R., and Arber, S. (2005). Hemojuvelin is essential for dietary iron sensing, and its mutation leads to severe iron overload. J. Clin. Invest. *115*, 2180–2186.

Nishiyama, M., Oshikawa, K., Tsukada, Y., Nakagawa, T., Iemura, S., Natsume, T., Fan, Y., Kikuchi, A., Skoultchi, A.I., and Nakayama, K.I. (2009). CHD8 suppresses p53-mediated apoptosis through histone H1 recruitment during early embryogenesis. Nat. Cell Biol. *11*, 172–182.

Onoyama, I., Suzuki, A., Matsumoto, A., Tomita, K., Katagiri, H., Oike, Y., Nakayama, K., and Nakayama, K.I. (2011). Fbxw7 regulates lipid metabolism and cell fate decisions in the mouse liver. J. Clin. Invest. *121*, 342–354.

Postic, C., and Magnuson, M.A. (2000). DNA excision in liver by an albumin-Cre transgene occurs progressively with age. Genesis *26*, 149–150.

Recalcati, S., Alberghini, A., Campanella, A., Gianelli, U., De Camilli, E., Conte, D., and Cairo, G. (2006). Iron regulatory proteins 1 and 2 in human monocytes, macrophages and duodenum: expression and regulation in hereditary hemochromatosis and iron deficiency. Haematologica *91*, 303–310.

Rouault, T.A., and Tong, W.H. (2005). Iron-sulphur cluster biogenesis and mitochondrial iron homeostasis. Nat. Rev. Mol. Cell Biol. *6*, 345–351.

Salahudeen, A.A., Thompson, J.W., Ruiz, J.C., Ma, H.W., Kinch, L.N., Li, Q., Grishin, N.V., and Bruick, R.K. (2009). An E3 ligase possessing an iron-responsive hemerythrin domain is a regulator of iron homeostasis. Science *326*, 722–726.

Sorrentino, P., D'Angelo, S., Ferbo, U., Micheli, P., Bracigliano, A., and Vecchione, R. (2009). Liver iron excess in patients with hepatocellular carcinoma developed on non-alcoholic steato-hepatitis. J. Hepatol. *50*, 351–357.

Vashisht, A.A., Zumbrennen, K.B., Huang, X., Powers, D.N., Durazo, A., Sun, D., Bhaskaran, N., Persson, A., Uhlen, M., Sangfelt, O., et al. (2009). Control of iron homeostasis by an iron-regulated ubiquitin ligase. Science *326*, 718–721.

Wang, J., and Pantopoulos, K. (2011). Regulation of cellular iron metabolism. Biochem. J. *434*, 365–381.

Zhang, N., Liu, J., Ding, X., Aikhionbare, F., Jin, C., and Yao, X. (2007). FBXL5 interacts with p150^{Glued} and regulates its ubiquitination. Biochem. Biophys. Res. Commun. *359*, 34–39.

Zhou, X.Y., Tomatsu, S., Fleming, R.E., Parkkila, S., Waheed, A., Jiang, J., Fei, Y., Brunt, E.M., Ruddy, D.A., Prass, C.E., et al. (1998). HFE gene knockout produces mouse model of hereditary hemochromatosis. Proc. Natl. Acad. Sci. USA *95*, 2492–2497.

Cell Stem Cell
Short Article

p57 Is Required for Quiescence and Maintenance of Adult Hematopoietic Stem Cells

Akinobu Matsumoto,[1,2] Shoichiro Takeishi,[1,2] Tomoharu Kanie,[1,2] Etsuo Susaki,[1,2] Ichiro Onoyama,[1,2] Yuki Tateishi,[1,2] Keiko Nakayama,[2,3] and Keiichi I. Nakayama[1,2,*]
[1]Department of Molecular and Cellular Biology, Medical Institute of Bioregulation, Kyushu University, 3-1-1 Maidashi, Higashi-ku, Fukuoka, Fukuoka 812-8582, Japan
[2]CREST, Japan Science and Technology Agency (JST), Kawaguchi, Saitama 332-0012, Japan
[3]Department of Developmental Genetics, Center for Translational and Advanced Animal Research, Graduate School of Medicine, Tohoku University, 2-1 Seiryo-machi, Aoba-ku, Sendai 980-8575, Japan
*Correspondence: nakayak1@bioreg.kyushu-u.ac.jp
DOI 10.1016/j.stem.2011.06.014

SUMMARY

Quiescence is required for the maintenance of hematopoietic stem cells (HSCs). Members of the Cip/Kip family of cyclin-dependent kinase (CDK) inhibitors (p21, p27, p57) have been implicated in HSC quiescence, but loss of p21 or p27 in mice affects HSC quiescence or functionality only under conditions of stress. Although p57 is the most abundant family member in quiescent HSCs, its role has remained uncharacterized. Here we show a severe defect in the self-renewal capacity of p57-deficient HSCs and a reduction of the proportion of the cells in G_0 phase. Additional ablation of p21 in a p57-null background resulted in a further decrease in the colony-forming activity of HSCs. Moreover, the HSC abnormalities of p57-deficient mice were corrected by knocking in the *p27* gene at the *p57* locus. Our results therefore suggest that, among Cip/Kip family CDK inhibitors, p57 plays a predominant role in the quiescence and maintenance of adult HSCs.

INTRODUCTION

Progression of the cell cycle is controlled by pairs of cyclins and cyclin-dependent kinases (CDKs). Progression through G_1 phase of the cell cycle is dependent on the cyclin D-CDK4 (or CDK6) complex, whereas cyclin E-CDK2 is required for the G_1-S transition and cyclins A and B together with CDK1 are required for G_2-M progression (Sherr and Roberts, 2004). Cell cycle progression is also under the control of negative regulators, the CDK inhibitors (CKIs), which belong to either the Ink4 or Cip/Kip families. Members of the Ink4 family—such as $p16^{Ink4a}$, $p15^{Ink4b}$, $p18^{Ink4c}$, and $p19^{Ink4d}$—are inhibitors specific for CDK4 or CDK6, whereas those of the Cip/Kip family, including $p21^{Cip1}$ (p21), $p27^{Kip1}$ (p27), and $p57^{Kip2}$ (p57), mainly target CDK2 and CDK4 (and CDK1 in some situations) for inhibition.

Sustained hematopoiesis in adults requires preservation of a quiescent, multipotential hematopoietic stem cell (HSC) pool that intermittently yields progenitors with robust proliferative potential (Arai and Suda, 2007). In contrast, the cell cycle of HSCs is active during embryogenesis in order to ensure expansion of the stem cell pool (Pawliuk et al., 1996). The ability of adult HSCs to reside in the quiescent state has been thought to be pivotal for maintenance of their "stemness." However, the precise mechanisms by which such quiescence is established, maintained, and terminated have been largely unknown. CKIs including p21, p27, and p57 are implicated in the maintenance of quiescence, given their function to antagonize CDK activity that promotes cell proliferation. However, self-renewal of HSCs in mice deficient in p21 was found to be impaired only under stressful conditions in which DNA is damaged by exposure to 5-fluorouracil or γ-irradiation (Cheng et al., 2000b; van Os et al., 2007). Deletion of p27 in mice also does not affect the number, cycling, or self-renewal of HSCs (Cheng et al., 2000a). Although many studies have suggested the importance of p57 for maintenance of HSC stemness (Miyamoto et al., 2007; Qian et al., 2007; Yamazaki et al., 2006), the role of p57 in control of HSC quiescence has remained poorly characterized. Unlike p21- or p27-deficient mice, mice lacking p57 die immediately after birth, manifesting severe developmental defects (Takahashi et al., 2000; Yan et al., 1997; Zhang et al., 1997), which has rendered functional characterization of their HSCs technically difficult.

We have now established mice in which the p57 gene is conditionally disrupted in the hematopoietic system in order to avoid the neonatal mortality of conventional p57-deficient mice. Deletion of p57 alone, but not that of p21 or p27, resulted in a reduction in HSC number, in the size of the G_0 population, and in their reconstitution ability after transplantation. Mice lacking both p21 and p57 showed a more severe phenotype than those lacking p57 alone, and knockin of the gene for p27 at the *p57* locus corrected the abnormalities of p57-deficient mice, suggestive of functional overlap between p57 and either p21 or p27. Our data thus indicate that p57 plays the dominant role among CKIs of the Cip/Kip family in maintenance of quiescence and stemness of HSCs.

RESULTS

p57 Is Predominantly Expressed in the Long-Term HSC Population

A previous study suggested that, among hematopoietic cells, p57 mRNA is most abundant in $CD34^-c\text{-}Kit^+Sca\text{-}1^+$ lineage marker-negative (Lin^-) HSCs ($CD34^-KSL$ HSCs), a fraction with

long-term repopulating capacity (Yamazaki et al., 2006). In contrast, p21 mRNA was not detected in CD34$^-$KSL HSCs, whereas p27 mRNA was found to be present in both CD34$^-$KSL and CD34$^+$KSL cells, the latter corresponding to a fraction with short-term repopulating capacity. To examine the expression of p57 in HSCs at the protein level, we performed immunoblot analysis of sorted bone marrow (BM) samples from 12 wild-type mice at 8 weeks of age. We sorted and fractionated KSL cells with the SLAM (signaling lymphocytic activation molecule) marker CD150. Similar to the pattern observed for its mRNA, p57 protein was most abundant in the CD150$^+$KSL fraction, a fraction with long-term repopulating capacity; it was present in smaller amounts in the CD150$^-$KSL fraction, a fraction with short-term repopulating capacity, and it was not detected in other fractions (Figure 1A). We did not detect p21 in any of the fractions tested, whereas p27 was expressed at a low level in the CD150$^+$KSL and CD150$^-$KSL populations. These patterns of protein expression prompted us to examine the effects of p57 ablation in HSCs.

Deletion of p57 Leads to a Reduction in Size of the HSC Population

Given that most conventional p57 knockout mice die during the perinatal period as a result of respiratory distress, probably caused by skeletal anomalies (Takahashi et al., 2000; Yan et al., 1997; Zhang et al., 1997), it has been technically difficult to characterize adult HSCs in such mice. We therefore established mouse embryonic stem cells (ESCs) that harbor a "floxed" *p57* allele in which exons 2 to 4 (which include the entire coding region) are flanked by loxP sites (see Figure S1A available online). This allele was generated by homologous recombination followed by transient transfection of the ESCs with a vector for Cre recombinase in order to remove the introduced *neo* cassette (Figure S1B). Mice heterozygous for the floxed allele (*p57*$^{+/F}$ mice) were generated by microinjection of the mutant ESCs into blastocysts and breeding of the resultant chimeric animals with mice of the C57BL/6 strain. The *p57* locus undergoes genomic imprinting, with only the maternal allele being expressed (Matsuoka et al., 1995). The *p57*$^{+/F}$ mice were indistinguishable from wild-type animals, confirming that the floxed allele is functional. We also confirmed that the phenotype of mice in which the maternal floxed allele was deleted by Cre recombinase expressed from the Ella gene promoter (Lakso et al., 1996) beginning early during embryogenesis was identical to that of conventional p57 knockout mice (Figure S1C). To ablate the maternal *p57* allele only in the hematopoietic system, we crossed female *p57*$^{+/F}$ mice with male mice harboring a Cre transgene under the control of the promoter for the myxovirus resistance 1 (Mx1) gene. We confirmed that almost all floxed alleles were inactivated by Cre recombinase in BM of Mx1-Cre/*p57*$^{+/F}$ mice after intraperitoneal injection of poly(I)-poly(C) [poly(I:C)] to activate the Mx1 gene promoter (Figure S1D). Without poly(I:C) injection, a slight decrease in the abundance of p57 mRNA was observed in Mx1-Cre/*p57*$^{+/F}$ mice compared with that in Mx1-Cre/*p57*$^{+/+}$ mice. Deletion of the *p57* allele resulted in a small increase in the amounts of p27 and p18 mRNAs in KSL cells, whereas deletion of p21 or p27 did not significantly affect the abundance of mRNAs for the corresponding other two CKIs (Figures S1E–S1H).

As early as 4 weeks after poly(I:C) injection, a substantial reduction in the size of the KSL fraction was apparent in p57-deficient mice compared with that in control littermates (Mx1-Cre/*p57*$^{+/+}$ mice), which were also injected with poly(I:C) to exclude the possibility that poly(I:C) affected phenotype regardless of genotype (Figure 1B). This reduction in the size of the KSL fraction in p57-deficient mice was apparent for all KSL subpopulations examined (CD150$^-$, CD150$^+$CD48$^-$, CD34$^-$, or CD34$^+$ cells) with the exception of CD150$^+$CD48$^+$ cells (Figure 1C). The total number and composition of cells in BM or peripheral blood were not otherwise affected by deletion of p57 at 4 weeks (Figures S1I–S1K and data not shown) or 4 months (Figure S1L and data not shown) after injection of poly(I:C), probably in part because the effect of such deletion in adult HSCs was compensated for at later stages of differentiation or had not had sufficient time to become manifest in the periphery within the period before analysis. In contrast, no reduction in the size of the HSC population was observed in p21- or p27-deficient mice (Figure 1C), consistent with the results of previous studies (Cheng et al., 2000a, 2000b; van Os et al., 2007). These findings thus suggested that p57 deletion affects the self-renewal capacity of HSCs.

Deletion of p57 Abrogates the Self-Renewal Capacity of HSCs

To assess the repopulating capacity of p57-deficient HSCs in vivo, we performed a competitive reconstitution assay in which BM cells (4×10^5) from poly(I:C)-injected Mx1-Cre/*p57*$^{+/+}$ or Mx1-Cre/*p57*$^{+/F}$ mice (CD45.2) competed against an equal number of BM cells from C57BL/6 heterozygous congenic mice (CD45.1/CD45.2) to reconstitute the hematopoietic compartment of irradiated C57BL/6 congenic mouse (CD45.1) recipients. At 16 weeks after BM cell transplantation (BMT), flow cytometric analysis of peripheral blood of the recipients revealed that the repopulating capacity of p57-deficient BM cells was markedly impaired, whereas that of *p21*$^{-/-}$ or *p27*$^{-/-}$ BM cells did not differ from that of cells from littermate controls (Figure 2A). Given that this result might have reflected the reduced number of HSCs in p57-deficient mice (Figures 1B and 1C), we also performed similar assays with total KSL cells (1.5×10^3) or CD150$^+$CD48$^-$KSL cells (2.0×10^2) isolated from p57-deficient mice or littermate controls at 4 weeks after poly(I:C) injection. The p57-deficient KSL cells showed a greatly impaired repopulating capacity after the first BMT, and this impairment was even more pronounced after a second BMT (Figures 2B and 2C). In addition, the frequency of KSL cells derived from p57-deficient donors among BM cells of the recipient mice was markedly smaller than that for KSL cells derived from control donors (Figure 2D). To determine whether p57 intrinsically regulates HSC repopulating capability, we transplanted BM cells (4×10^5) from either Mx1-Cre/*p57*$^{+/F}$ mice or littermate controls not treated with poly(I:C) into lethally irradiated recipients together with the same number of competitor cells. After 4 weeks, we confirmed that donor cells were reconstituted in recipient BM and then injected the recipient mice with poly(I:C). Within 1 month after poly(I:C) injection, p57-deficient HSCs lost long-term repopulating capability and were eventually competed out by wild-type HSCs (Figure 2E), suggesting that a homing defect of transferred BM cells probably was not responsible for the impaired BM reconstitution by p57-deficient HSCs.

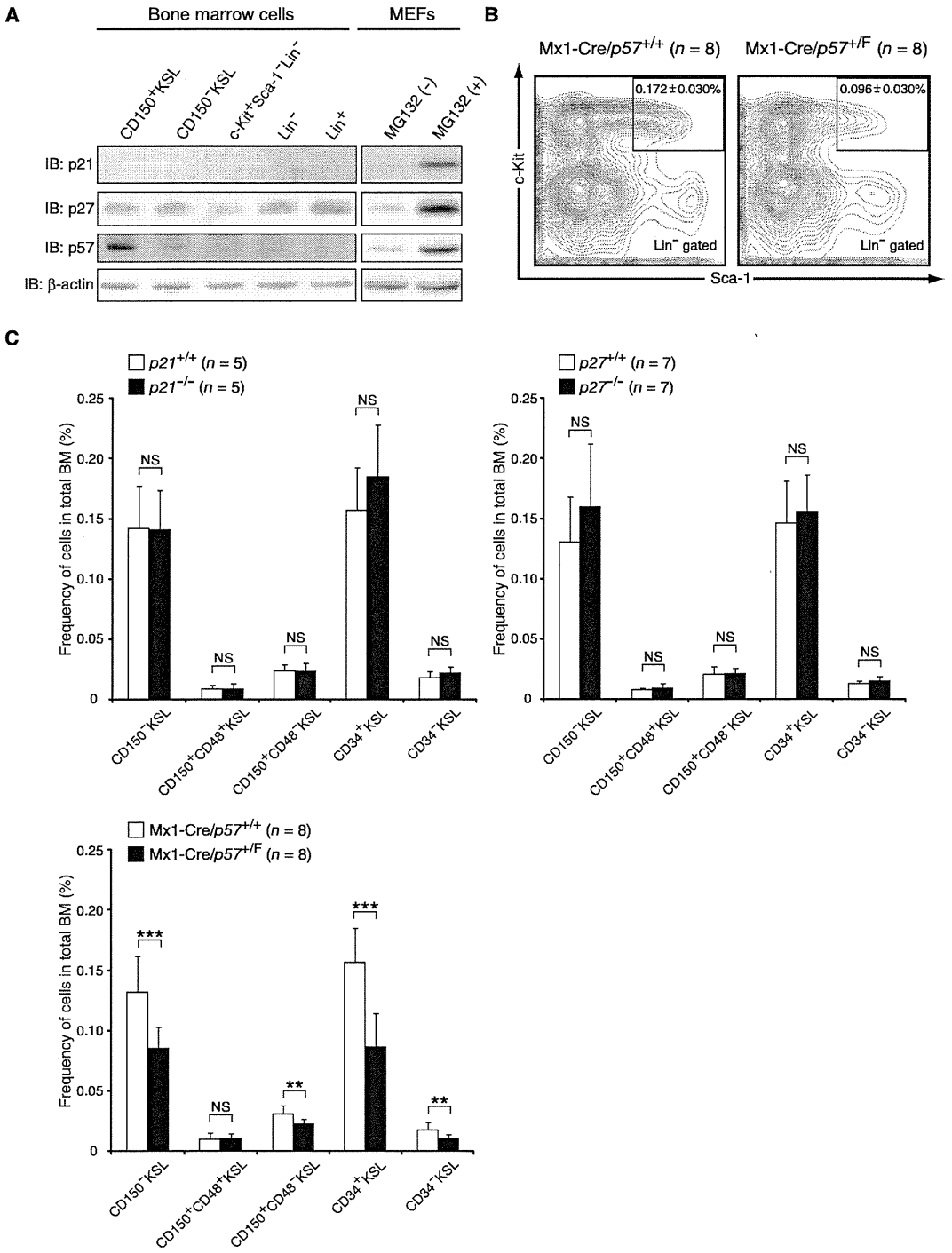

Figure 1. Decrease in HSC Number Induced by p57 Deletion

(A) Immunoblot analysis (IB) of fractionated hematopoietic cells from BM of wild-type mice. For positive and negative controls, mouse embryonic fibroblasts (MEFs) were cultured with or without 100 μM MG132, respectively.

(B) Flow cytometric determination of the frequency of KSL cells among BM cells of Mx1-Cre/$p57^{+/+}$ and Mx1-Cre/$p57^{+/F}$ mice at 4 weeks after poly(I:C) injection. The percentages of KSL cells among total BM cells are shown as means ± SD.

(C) Frequency of the indicated fractions among total BM cells from mice of the indicated genotypes. Mice harboring the Mx1-Cre transgene were examined at 4 weeks after poly(I:C) injection. Data are means ± SD. **$p < 0.01$, ***$p < 0.005$; NS, not significant.

See also Figure S1.

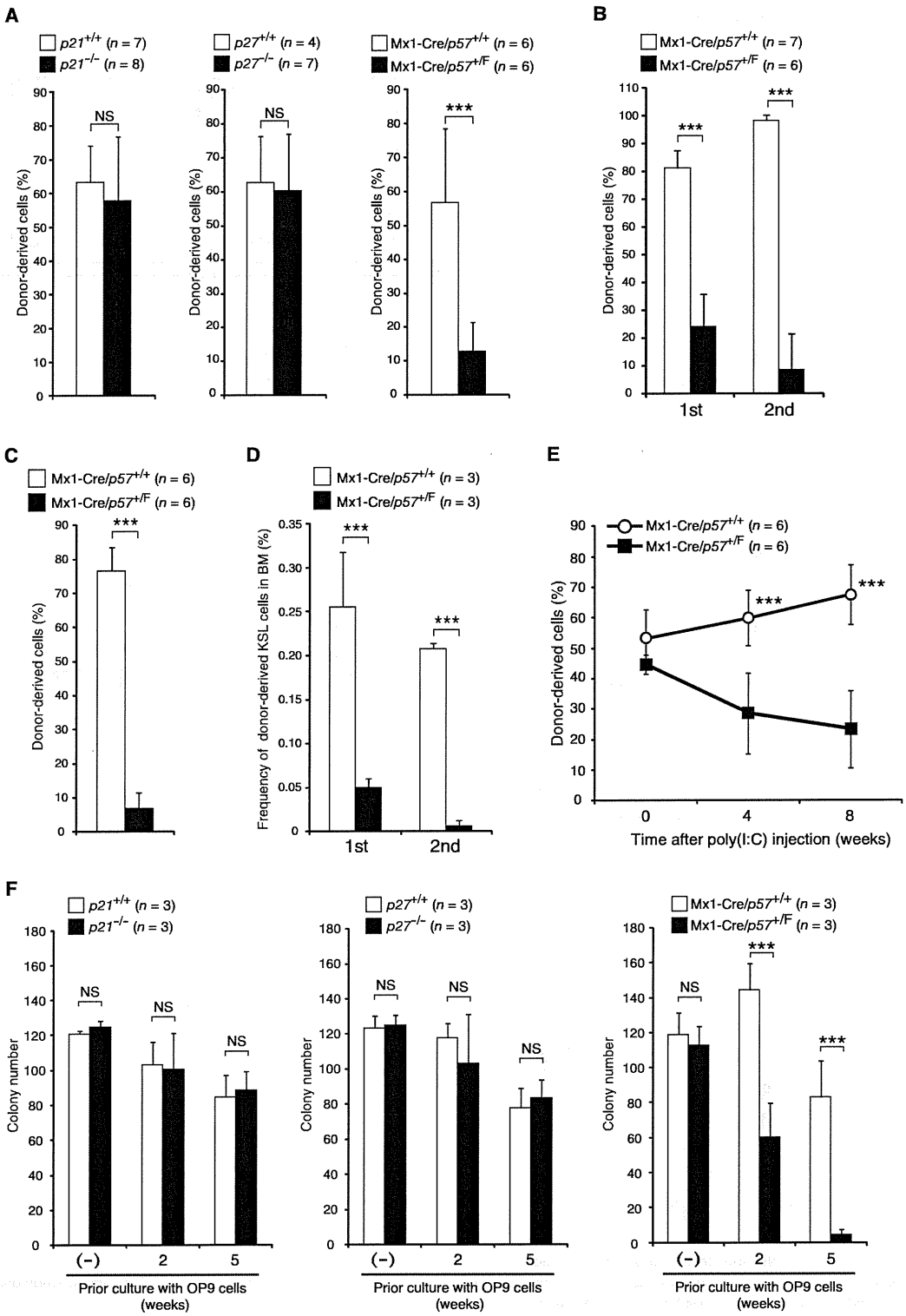

Figure 2. p57, but Not p21 or p27, Is Essential for HSC Maintenance

(A) Hematopoietic reconstitution capacity of BM cells (4×10^5) from donor mice of the indicated genotypes. Cells from donors harboring the Mx1-Cre transgene were harvested at 4 weeks after poly(I:C) injection. Data are means ± SD. ***$p < 0.005$.

We further performed long-term culture of KSL cells on a layer of OP9 stromal cells, with the number of colony-forming cells arising after 2 or 5 weeks of culture reflecting the function of hematopoietic progenitor or stem cells, respectively. The number of colonies derived from p57-deficient KSL cells was significantly decreased compared with that derived from control cells, although a similar assay with freshly isolated KSL cells without culture did not show a significant difference in the number of colonies formed (Figure 2F). The number of colonies derived from p21- or p27-deficient KSL cells did not differ significantly from that derived from the corresponding control cells with or without culture on OP9 cells. A serial replating assay revealed that the number of colonies derived from p57-deficient KSL cells declined to a greater extent compared with that of colonies derived from control cells with each plating, whereas the number of colonies derived from p21- or p27-deficient KSL cells did not differ significantly from that derived from the corresponding control cells at each plating (Figure S2). Collectively, these results suggested that the self-renewal capacity of HSCs was profoundly affected by the loss of p57, but not by that of p21 or p27.

p57 Is Required for Maintenance of Quiescence in HSCs

HSCs are normally maintained in an undifferentiated quiescent (G_0 phase) state, with this quiescence protecting the cells against loss of self-renewal capacity. To evaluate directly HSC quiescence in p57-deficient mice, we stained KSL cells from poly(I:C)-injected Mx1-Cre/$p57^{+/+}$ or Mx1-Cre/$p57^{+/F}$ mice with a combination of Hoechst 33342 and pyronin Y, which differentially and quantitatively stain DNA and RNA and thereby allow detection of cells in G_0 phase. We found that 28% of control KSL cells were negative for staining with pyronin Y, indicative of normal HSC quiescence, whereas only 15% of p57-deficient KSL cells were in G_0 phase (Figures 3A and 3B). No such difference was observed for p21- or p27-deficient KSL cells and the corresponding control cells. We also examined the cell cycle status of $CD34^-$KSL and $CD34^+$KSL cells on the basis of 5-bromodeoxyuridine (BrdU) incorporation. More $BrdU^+$ cells were detected among p57-deficient $CD34^-$KSL and $CD34^+$KSL populations than among the corresponding control cells (Figure 3C), consistent with the reduced size of the G_0 population for p57-deficient KSL cells. Furthermore, the frequency of apoptosis was substantially increased among p57-deficient KSL cells, but not among p21- or p27-deficient KSL cells (Figure 3D). Similar results were obtained 3 days after the onset of a shortened course of poly(I:C) treatment (Figures S3A–S3D). These results thus suggested that p57, but not p21 or p27, is essential for maintenance of HSC quiescence.

Immunofluoresence analysis revealed that the expression of p53 was increased in p57-deficient KSL cells (Figures S3E and S3F). Treatment of p57-deficient cells with the p53 inhibitor pifithrin-α resulted in suppression of apoptosis and significant restoration of their colony-forming ability (Figures S3G and S3H). Phosphorylation of the retinoblastoma protein (Rb) was increased in p57-deficient KSL cells compared with that in control cells, whereas no such difference was observed between the c-$Kit^+Sca\text{-}1^-Lin^-$ populations of the two genotypes (Figures 3E–3G). Treatment of p57-deficient KSL cells with the chemical CDK inhibitor SU9516, which is relatively specific for CDK2, reversed, at least in part, the changes in colony-forming ability, quiescence, and viability induced by loss of p57 (Figures 3H–3K), suggesting that increased CDK activity contributes to these effects of p57 deletion in KSL cells. Collectively, these results indicated that the loss of p57 results in exhaustion of HSCs, which is attributable in part to the induction of apoptosis mediated by upregulation of CDK activity and p53 expression.

Functional Overlap of p57 with Other CKIs

Although our data indicated that p57 is a key CKI in the determination of stemness of HSCs, it remained possible that other CKIs might partially compensate for the effects of p57 deficiency. To examine this possibility, we generated double-mutant mice that lack both p21 and p57 (Mx1-Cre/$p21^{-/-}$/$p57^{+/F}$ mice injected with poly(I:C)). Whereas deletion of p57 alone did not affect colony-forming activity of KSL cells in vitro before coculture with OP9 cells (Figure 2F), combined deletion of p21 and p57 resulted in a decrease in such colony formation (Figure 4A). Furthermore, the size of individual colonies was markedly smaller for the double mutant cells than for cells of poly(I:C)-injected Mx1-Cre/$p21^{+/+}$/$p57^{+/+}$ or Mx1-Cre/$p21^{+/+}$/$p57^{+/F}$ mice (Figure 4B). The number of colonies formed after coculture with OP9 cells was further decreased for the double-mutant KSL cells compared with that for p57-deficient KSL cells (Figure 4C). However, no significant difference in the percentage of cells in G_0 phase or in the frequency of apoptosis was apparent between KSL cells deficient in p57 alone and those deficient in both p21 and p57 (Figures 4D and 4E). Together, these results suggested that the combined deletion of both CKIs might affect not only HSCs but also progenitor cells. We also examined HSC function in mice lacking both p21 and p27. The number of colonies formed, the percentage of cells in quiescence, and the frequency of apoptosis did not differ significantly between KSL cells derived from $p21^{-/-}$/$p27^{-/-}$ mice and those derived from wild-type mice (Figures S4A–S4C).

Whereas the members of the Cip/Kip family of CKIs (p21, p27, p57) share a CKI domain that is essential for inhibition of CDKs,

(B and C) Hematopoietic reconstitution capacity of KSL cells (1.5×10^3) (B) or $CD150^+CD48^-$KSL cells (2×10^2) (C) derived from Mx1-Cre/$p57^{+/F}$ or control donor mice at 4 weeks after poly(I:C) injection. BM cells (2×10^6) from the recipient mice in (B) were serially transplanted into additional recipient mice. Data are means ± SD. ***$p < 0.005$.

(D) Frequency of donor-derived KSL cells among total BM cells of recipient mice in (B) at 16 weeks after transplantation. Data are means ± SD. ***$p < 0.005$.

(E) Irradiated recipient mice were transplanted with donor BM cells (4×10^5) from Mx1-Cre/$p57^{+/+}$ or Mx1-Cre/$p57^{+/F}$ mice (not injected with poly(I:C)) together with an equal number of competitor BM cells. The recipients were injected with poly(I:C) at 4 weeks after transplantation, and the percentage of donor-derived cells in peripheral blood was determined. Data are means ± SD. ***$p < 0.005$.

(F) In vitro colony formation capacity of KSL cells from mice of the indicated genotypes with or without prior coculture with OP9 cells. Cells from mice harboring the Mx1-Cre transgene were harvested at 4 weeks after poly(I:C) injection. Data are means ± SD. ***$p < 0.005$.

See also Figure S2.

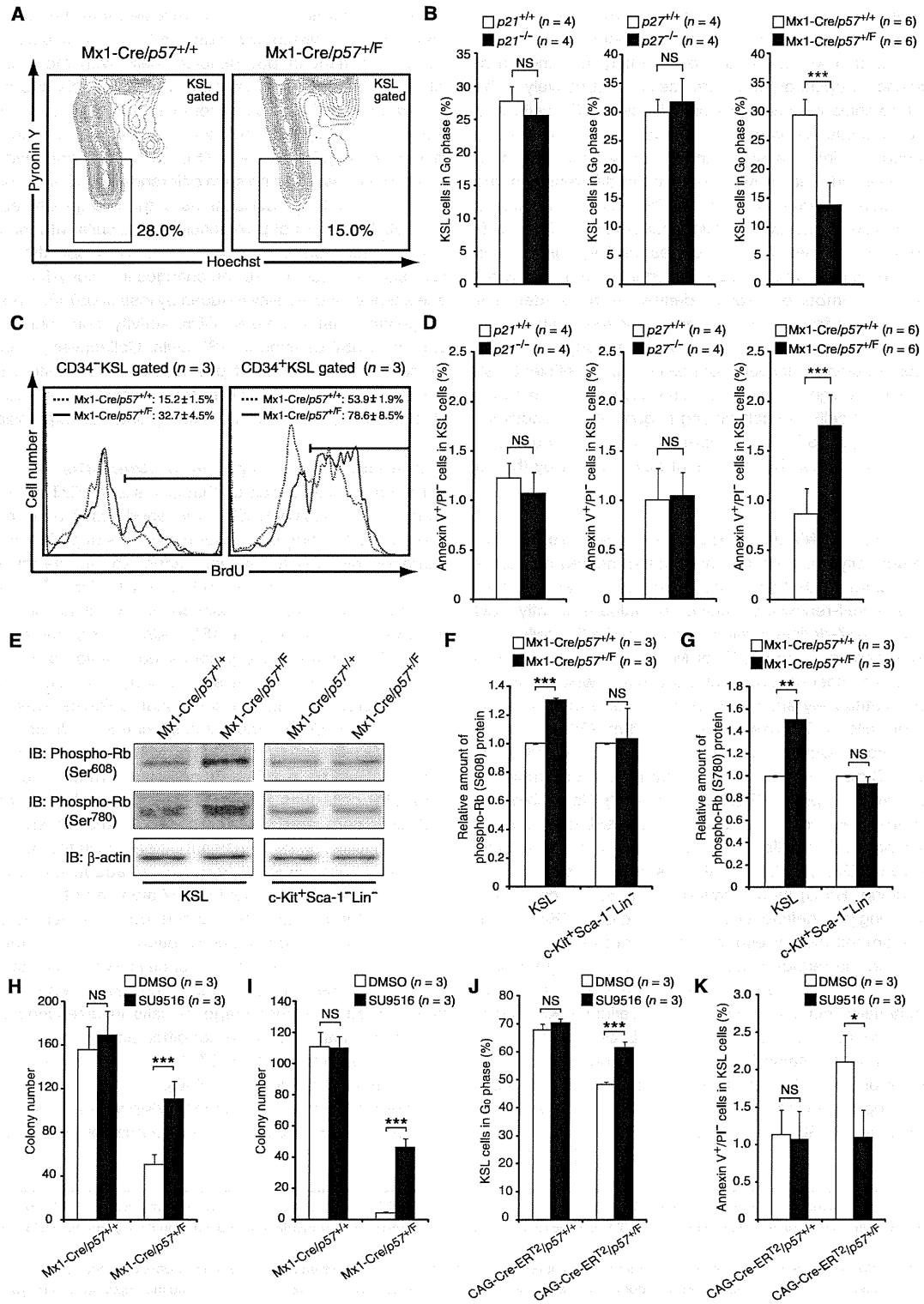

Figure 3. Loss of Quiescence and Induction of Apoptosis due to Increased CDK Activity in p57-Deficient HSCs

(A) Frequency of quiescence in KSL cells of Mx1-Cre/$p57^{+/+}$ and Mx1-Cre/$p57^{+/F}$ mice at 4 weeks after poly(I:C) injection. Quiescent cells were detected by staining with Hoechst 33342 and pyronin Y followed by flow cytometry.

p57 also contains a central domain that is absent in p21 and p27 and is thought to mediate functions other than inhibition of CDKs (Matsuoka et al., 1995). To test whether p57 function in the maintenance of HSCs is replaceable by p27, we examined the BM of $p57^{p27KI}$ mice, in which the p57 gene has been replaced with the p27 gene (Susaki et al., 2009). Similar to the pattern of p57 expression in wild-type mice, HA-tagged p27 encoded by the knockin allele at the p57 gene locus was expressed only in the KSL fraction, not in other more differentiated cells (Figure 4F). The size of the KSL population in $p57^{p27KI}$ mice was indistinguishable from that in wild-type mice (Figure 4G), and there was no difference in repopulating capacity at the first BMT, in colony formation in vitro with or without prior coculture with OP9 cells, or in the frequency of quiescence or apoptosis between HSCs of the two genotypes (Figures 4H–4K; Figure S4D). These results suggested that the total abundance of CKIs of the Cip/Kip family is an important determinant of HSC stemness.

DISCUSSION

We have examined the physiological importance of p57 in maintenance of HSCs by analysis of the effects of conditional deletion of p57 in mouse hematopoietic cells. Such mice lacking p57 manifested a reduction in the size of the HSC fraction as well as in the self-renewal capacity and G_0 population of KSL cells, effects that were not observed in mice lacking p21 or p27 (or both). We thus conclude that p57 plays the dominant role among Cip/Kip CKIs in the maintenance of HSCs.

The related CKIs p27 and p57 differ in the spatiotemporal patterns of their expression in many tissues and organs (Nagahama et al., 2001). Whereas p57 is most abundant in the HSC fraction of BM cells, its expression ceases as HSCs differentiate into progenitor cells. Expression of p27 is apparent in all hematopoietic fractions, whereas p21 is not detected in such cells in the absence of genotoxic stress. The expression patterns of these CKIs appear consistent with the phenotypes of the corresponding knockout mice. However, our present results suggest the existence of functional overlap between p57 and its related CKIs. The defects induced by p57 deficiency were thus reversed by p27 knockin, suggesting that the function of these CKIs at the molecular level is indistinguishable. We hypothesize that the specific response of cells to the lack of each CKI might be dependent on the total CKI abundance rather than on CKI type, but further investigation will be necessary to confirm this hypothesis. This relation between p27 and p57 in HSCs is similar to that observed in most (but not all) other tissues examined (Susaki et al., 2009).

Regulation of the cell cycle is thought to play a key role in the maintenance and function of HSCs. Mutant mice with deletions in genes for various cell cycle regulators thus manifest defects in HSC maintenance and function. The numbers of HSCs as well as common myeloid and lymphoid progenitors are decreased in mice with conditional inactivation of cyclin A2 (Kalaszczynska et al., 2009). The reconstitution ability of BM cells is also markedly impaired in these latter mutant mice. Likewise, mice lacking all D-type cyclins (cyclins D1, D2, and D3) show pronounced BM defects associated with a loss of the reconstitution capacity of BM cells; these animals develop severe anemia and die in utero (Kozar et al., 2004). Similar defects are apparent in mice deficient in both CDK4 and CDK6, which are the major partners of D-type cyclins (Malumbres et al., 2004). In contrast, no abnormality is apparent in mice lacking CDK2 (Berthet et al., 2007), suggesting that CDK1 may compensate for the loss of CDK2 (Aleem et al., 2005).

Rb is a major target of CDK2 and CDK4. Vav1-Cre/$Rb^{F/F}$ mice, which express Cre recombinase in hematopoietic cells, show a marked defect in the self-renewal competence and multipotency of HSCs (Daria et al., 2008), and deletion of all members of the Rb family (Rb, p107, and p130) further exacerbated this phenotype (Viatour et al., 2008). Mice deficient in E2F1, E2F2, and E2F3, all of which are downstream targets of Rb, show a decrease in the number of myeloid cells but maintain the function of HSCs (Viatour et al., 2008).

Some of the members of the Ink4 family of CKIs also contribute to the regulation of HSCs. Expression of $p16^{Ink4a}$ in HSCs increases with age, and the self-renewal capacity of HSCs does not decline with age in mice deficient in this CKI (Janzen et al., 2006). Mice lacking $p15^{Ink4b}$ do not exhibit an apparent defect in HSC function, although the proliferation of progenitors for granulocytes and monocytes is enhanced in these animals (Rosu-Myles et al., 2007). Loss of $p18^{Ink4c}$ results in expansion of the HSC pool associated with promotion of the cell cycle without loss of self-renewal capacity (Yuan et al., 2004). The effects of deletion of Ink4 CKIs thus appear opposite to those of deletion of Cip/Kip CKIs. Deletion of Cip/Kip CKIs results in

(B) Quantitative analysis of quiescent cells among KSL cells from mice of the indicated genotypes as determined from experiments similar to that in (A). Data are means ± SD. ***$p < 0.005$.

(C) Frequency of proliferating cells among $CD34^-$KSL and $CD34^+$KSL cells isolated from Mx1-Cre/$p57^{+/+}$ and Mx1-Cre/$p57^{+/F}$ mice at 4 weeks after poly(I:C) injection. Proliferating cells were detected by BrdU pulse-labeling analysis in vivo. The percentages of BrdU-positive cells are indicated as means ± SD.

(D) Quantitative analysis of apoptotic cells among KSL cells from mice of the indicated genotypes. Apoptotic cells in the KSL fraction were detected by staining with annexin V and propidium iodide (PI). Data are means ± SD. ***$p < 0.005$.

(E) Immunoblot analysis of phosphorylated Rb in KSL and c-$Kit^+Sca\text{-}1^-Lin^-$ cells from Mx1-Cre/$p57^{+/+}$ and Mx1-Cre/$p57^{+/F}$ mice at 4 weeks after poly(I:C) injection.

(F and G) Quantitative analysis of the relative amounts of Ser608-phosphorylated Rb (F) and Ser780-phosphorylated Rb (G) as determined from experiments similar to that in (E). Data are means ± SD. **$p < 0.01$, ***$p < 0.005$.

(H and I) Colony formation by KSL cells from Mx1-Cre/$p57^{+/+}$ and Mx1-Cre/$p57^{+/F}$ mice at 4 weeks after poly(I:C) injection after coculture on OP9 cells for 2 weeks (H) or 5 weeks (I) with 160 nM SU9516 or dimethyl sulfoxide (DMSO). Data are means ± SD. ***$p < 0.005$.

(J and K) Quantitative analysis of quiescent cells (J) and apoptotic cells (K) among KSL cells from CAG-Cre-ER^{T2}/$p57^{+/+}$ and CAG-Cre-ER^{T2}/$p57^{+/F}$ mice after culture for 2 weeks on OP9 cells, the second week in the presence of 1 μM 4-hydroxytamoxifen (4-OHT) and either 160 nM SU9516 or DMSO. Data are means ± SD. ***$p < 0.005$.

See also Figure S3.

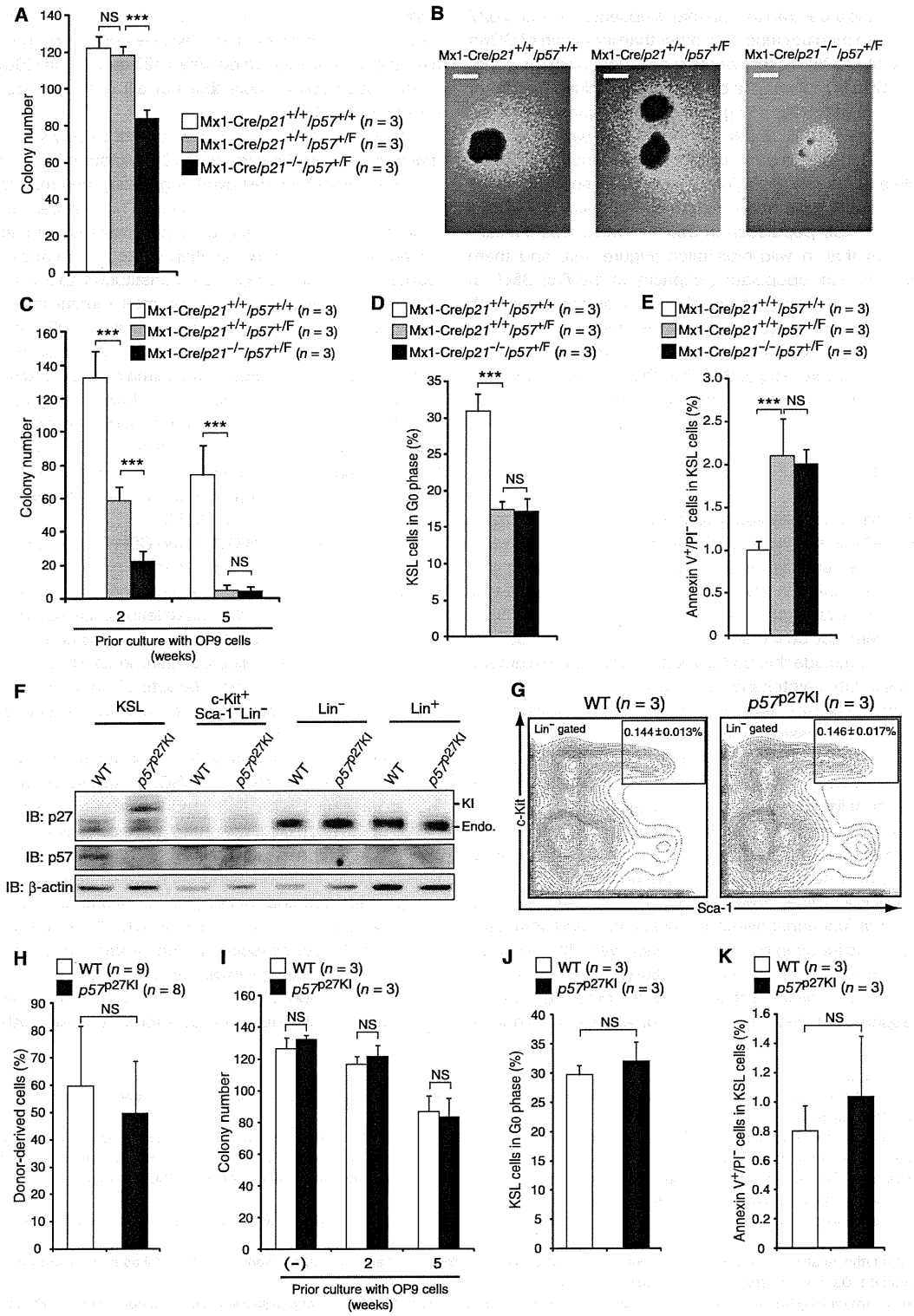

Figure 4. Overlap of CKI Function in HSC Maintenance

(A) In vitro colony formation capacity of KSL cells from mice of the indicated genotypes at 4 weeks after poly(I:C) injection. Data are means ± SD. ***$p < 0.005$.

(B) Representative colonies from the experiment shown in (A). Scale bars represent 0.5 mm.

exit of HSCs from the quiescent state and their entry into the proliferation cycle, an effect that is associated with the loss of self-renewal capacity or promotion of differentiation (or both).

The direct downstream targets of p27 and p57 CKIs are thought to be CDK2 and CDK4 (or CDK6), and inhibition of CDK activity by these CKIs maintains Rb in the unphosphorylated state (Halaban, 2005). Our results now show that the phosphorylation of Rb on Ser608 (phosphorylated by CDK2-cyclin A or E and CDK4-cyclin D) and Ser780 (phosphorylated by CDK4-cyclin D) (Halaban, 2005) was increased in p57-deficient KSL cells, suggesting that the activity of CDK2 or CDK4 (or both) is increased in KSL cells by deletion of p57.

We examined whether the effects of p57 deletion in HSCs are reversed by inhibition of CDK activity with the use of the chemical CDK inhibitor SU9516, which is relatively specific for CDK2 (Moshinsky et al., 2003). The in vitro colony formation capacity of KSL cells from poly(I:C)-injected Mx1-Cre/$p57^{+/F}$ mice was partially restored by treatment with SU9516 during prior coculture with OP9 cells, suggesting that increased activity of CDK2 is probably responsible for the effects of p57 deletion in KSL cells. The partial, rather than complete, restoration might be attributable to a contribution of CDK4 to the downregulation of colony formation ability in the p57-deficient KSL cells.

We have also shown that treatment of p57-deficient KSL cells with the p53 inhibitor pifithrin-α suppressed apoptosis and partially restored colony-forming ability. Furthermore, we have independently demonstrated that ablation of p57 results in hyperactivation of E2F1 and consequent p53-mediated apoptosis in mice (Susaki et al., 2009). Together, these lines of evidence support the notion that p57 deficiency results in abnormal upregulation of CDK activity, leading to hyperactivation of E2F1 and the triggering of p53-dependent apoptosis.

One of the substantial differences between fetal and adult HSCs is their dependency on quiescence: Maintenance of quiescence is thus thought to be more important for adult HSCs than for fetal HSCs. In an accompanying paper (Zou et al., 2011 [this issue of *Cell Stem Cell*]), HSCs in the fetal liver of conventional p27- or p57-deficient mice (Nakayama et al., 1996; Takahashi et al., 2000) were analyzed. Fetal HSCs lacking p57 did not manifest an apparent defect with the exception of a slight decrease in BM reconstitution capacity that was observed only after the third round of BM transfer. Combined deletion of p27 and p57 resulted in a marked failure in the maintenance of fetal HSCs, however, suggesting that these two CKIs have redundant roles. In contrast, our present study shows that p57 deficiency alone results in a substantial decrease in the number of adult HSCs as a result of their exit from quiescence and entry into apoptosis, with the BM reconstitution capacity of these p57-deficient cells also being greatly reduced from the first round of BM transfer. Deletion of p21 or p27 (or both proteins) did not result in any overt abnormalities in adult HSCs. Our analysis of mice lacking both p21 and p57 suggests that p21 also contributes to the maintenance of hematopoiesis, and that of $p57^{p27KI}$ mice suggests that p57 function in HSC maintenance can be replaced by p27. Collectively, our present study demonstrates that p57 plays a predominant role in constitutive maintenance of HSCs after birth.

EXPERIMENTAL PROCEDURES

Mice

Detailed methods for the generation of mice heterozygous for the floxed *p57* allele ($p57^{+/F}$ mice) as well as other mice used in this study are described in Supplemental Experimental Procedures. All mice were backcrossed with C57BL/6 mice more than six times. All mouse experiments were approved by the animal ethics committee of Kyushu University.

BM Reconstitution Assays

Unfractionated BM cells (4×10^5), sorted LSK cells (1.5×10^3), or sorted $CD150^+CD48^-$LSK cells (2×10^2) from $p21^{-/-}$, $p27^{-/-}$, Mx1-Cre/$p57^{+/F}$, or corresponding littermate control mice (CD45.2) were transplanted into lethally irradiated C57BL/6 congenic (CD45.1) recipients together with competitor BM cells (4×10^5) from C57BL/6 heterozygous congenic (CD45.1/CD45.2) mice. For serial transplantation analysis, BM cells (2×10^6) were obtained from recipient mice at 16 weeks after transplantation (first BMT) and were transferred to a second set of lethally irradiated mice (second BMT).

Colony Formation Assays

Sorted KSL cells were subjected to colony formation assays with or without prior coculture with OP9 cells. Detailed methods for the assays are described in Supplemental Experimental Procedures.

SUPPLEMENTAL INFORMATION

Supplemental Information includes Supplemental Experimental Procedures and four figures and can be found with this article online at doi:10.1016/j.stem.2011.06.014.

ACKNOWLEDGMENTS

We thank P. Leder for p21-deficient mice, Y. Fukui for Ella-Cre transgenic mice, D.R. Littman for pL2-Neo and pMC-Cre, T. Suda for sharing unpublished results, and Y. Matsuzaki, K. Shibata, A. Niihara, C. Mitai, Y. Yamada, K. Takeda, and M. Tanaka for technical assistance.

Received: December 13, 2010
Revised: June 1, 2011
Accepted: June 27, 2011
Published: September 1, 2011

(C) In vitro colony formation capacity of KSL cells from mice of the indicated genotypes after coculture with OP9 cells. Data are means ± SD. ***$p < 0.005$.
(D and E) Quantitative analysis of quiescent cells (D) and apoptotic cells (E) among KSL cells from mice of the indicated genotypes. Data are means ± SD. ***$p < 0.005$.
(F) Immunoblot analysis of fractionated hematopoietic cells from BM of wild-type (WT) and $p57^{p27KI}$ mice. The band positions for endogenous p27 (Endo.) and knocked-in hemagglutinin epitope-tagged p27 (KI) are shown.
(G) Frequency of KSL cells among BM cells of wild-type and $p57^{p27KI}$ mice. The percentages of KSL cells among total BM cells are shown as means ± SD.
(H) Hematopoietic reconstitution capacity of BM cells from $p57^{p27KI}$ and littermate control mice. Data are means ± SD.
(I) In vitro colony formation capacity of KSL cells from wild-type and $p57^{p27KI}$ mice with or without prior coculture with OP9 cells. Data are means ± SD.
(J and K) Quantitative analysis of quiescent cells (I) and apoptotic cells (J) among KSL cells from wild-type and $p57^{p27KI}$ mice. Data are means ± SD.
See also Figure S4.

REFERENCES

Aleem, E., Kiyokawa, H., and Kaldis, P. (2005). Cdc2-cyclin E complexes regulate the G1/S phase transition. Nat. Cell Biol. *7*, 831–836.

Arai, F., and Suda, T. (2007). Maintenance of quiescent hematopoietic stem cells in the osteoblastic niche. Ann. N Y Acad. Sci. *1106*, 41–53.

Berthet, C., Rodriguez-Galan, M.C., Hodge, D.L., Gooya, J., Pascal, V., Young, H.A., Keller, J., Bosselut, R., and Kaldis, P. (2007). Hematopoiesis and thymic apoptosis are not affected by the loss of Cdk2. Mol. Cell. Biol. *27*, 5079–5089.

Cheng, T., Rodrigues, N., Dombkowski, D., Stier, S., and Scadden, D.T. (2000a). Stem cell repopulation efficiency but not pool size is governed by $p27^{kip1}$. Nat. Med. *6*, 1235–1240.

Cheng, T., Rodrigues, N., Shen, H., Yang, Y., Dombkowski, D., Sykes, M., and Scadden, D.T. (2000b). Hematopoietic stem cell quiescence maintained by $p21^{cip1/waf1}$. Science *287*, 1804–1808.

Daria, D., Filippi, M.D., Knudsen, E.S., Faccio, R., Li, Z., Kalfa, T., and Geiger, H. (2008). The retinoblastoma tumor suppressor is a critical intrinsic regulator for hematopoietic stem and progenitor cells under stress. Blood *111*, 1894–1902.

Halaban, R. (2005). Rb/E2F: A two-edged sword in the melanocytic system. Cancer Metastasis Rev. *24*, 339–356.

Janzen, V., Forkert, R., Fleming, H.E., Saito, Y., Waring, M.T., Dombkowski, D.M., Cheng, T., DePinho, R.A., Sharpless, N.E., and Scadden, D.T. (2006). Stem-cell ageing modified by the cyclin-dependent kinase inhibitor $p16^{INK4a}$. Nature *443*, 421–426.

Kalaszczynska, I., Geng, Y., Iino, T., Mizuno, S., Choi, Y., Kondratiuk, I., Silver, D.P., Wolgemuth, D.J., Akashi, K., and Sicinski, P. (2009). Cyclin A is redundant in fibroblasts but essential in hematopoietic and embryonic stem cells. Cell *138*, 352–365.

Kozar, K., Ciemerych, M.A., Rebel, V.I., Shigematsu, H., Zagozdzon, A., Sicinska, E., Geng, Y., Yu, Q., Bhattacharya, S., Bronson, R.T., et al. (2004). Mouse development and cell proliferation in the absence of D-cyclins. Cell *118*, 477–491.

Lakso, M., Pichel, J.G., Gorman, J.R., Sauer, B., Okamoto, Y., Lee, E., Alt, F.W., and Westphal, H. (1996). Efficient in vivo manipulation of mouse genomic sequences at the zygote stage. Proc. Natl. Acad. Sci. USA *93*, 5860–5865.

Malumbres, M., Sotillo, R., Santamaría, D., Galán, J., Cerezo, A., Ortega, S., Dubus, P., and Barbacid, M. (2004). Mammalian cells cycle without the D-type cyclin-dependent kinases Cdk4 and Cdk6. Cell *118*, 493–504.

Matsuoka, S., Edwards, M.C., Bai, C., Parker, S., Zhang, P., Baldini, A., Harper, J.W., and Elledge, S.J. (1995). $p57^{KIP2}$, a structurally distinct member of the $p21^{CIP1}$ Cdk inhibitor family, is a candidate tumor suppressor gene. Genes Dev. *9*, 650–662.

Miyamoto, K., Araki, K.Y., Naka, K., Arai, F., Takubo, K., Yamazaki, S., Matsuoka, S., Miyamoto, T., Ito, K., Ohmura, M., et al. (2007). Foxo3a is essential for maintenance of the hematopoietic stem cell pool. Cell Stem Cell *1*, 101–112.

Moshinsky, D.J., Bellamacina, C.R., Boisvert, D.C., Huang, P., Hui, T., Jancarik, J., Kim, S.H., and Rice, A.G. (2003). SU9516: Biochemical analysis of cdk inhibition and crystal structure in complex with cdk2. Biochem. Biophys. Res. Commun. *310*, 1026–1031.

Nagahama, H., Hatakeyama, S., Nakayama, K., Nagata, M., Tomita, K., and Nakayama, K. (2001). Spatial and temporal expression patterns of the cyclin-dependent kinase (CDK) inhibitors $p27^{Kip1}$ and $p57^{Kip2}$ during mouse development. Anat. Embryol. (Berl.) *203*, 77–87.

Nakayama, K., Ishida, N., Shirane, M., Inomata, A., Inoue, T., Shishido, N., Horii, I., Loh, D.Y., and Nakayama, K.I. (1996). Mice lacking $p27^{Kip1}$ display increased body size, multiple organ hyperplasia, retinal dysplasia, and pituitary tumors. Cell *85*, 707–720.

Pawliuk, R., Eaves, C., and Humphries, R.K. (1996). Evidence of both ontogeny and transplant dose-regulated expansion of hematopoietic stem cells in vivo. Blood *88*, 2852–2858.

Qian, H., Buza-Vidas, N., Hyland, C.D., Jensen, C.T., Antonchuk, J., Månsson, R., Thoren, L.A., Ekblom, M., Alexander, W.S., and Jacobsen, S.E.W. (2007). Critical role of thrombopoietin in maintaining adult quiescent hematopoietic stem cells. Cell Stem Cell *1*, 671–684.

Rosu-Myles, M., Taylor, B.J., and Wolff, L. (2007). Loss of the tumor suppressor $p15^{Ink4b}$ enhances myeloid progenitor formation from common myeloid progenitors. Exp. Hematol. *35*, 394–406.

Sherr, C.J., and Roberts, J.M. (2004). Living with or without cyclins and cyclin-dependent kinases. Genes Dev. *18*, 2699–2711.

Susaki, E., Nakayama, K., Yamasaki, L., and Nakayama, K.I. (2009). Common and specific roles of the related CDK inhibitors p27 and p57 revealed by a knock-in mouse model. Proc. Natl. Acad. Sci. USA *106*, 5192–5197.

Takahashi, K., Nakayama, K., and Nakayama, K.I. (2000). Mice lacking a CDK inhibitor, $p57^{Kip2}$, exhibit skeletal abnormalities and growth retardation. J. Biochem. *127*, 73–83.

van Os, R., Kamminga, L.M., Ausema, A., Bystrykh, L.V., Draijer, D.P., van Pelt, K., Dontje, B., and de Haan, G. (2007). A limited role for $p21^{Cip1/Waf1}$ in maintaining normal hematopoietic stem cell functioning. Stem Cells *25*, 836–843.

Viatour, P., Somervaille, T.C., Venkatasubrahmanyam, S., Kogan, S., McLaughlin, M.E., Weissman, I.L., Butte, A.J., Passegué, E., and Sage, J. (2008). Hematopoietic stem cell quiescence is maintained by compound contributions of the retinoblastoma gene family. Cell Stem Cell *3*, 416–428.

Yamazaki, S., Iwama, A., Takayanagi, S.I., Morita, Y., Eto, K., Ema, H., and Nakauchi, H. (2006). Cytokine signals modulated via lipid rafts mimic niche signals and induce hibernation in hematopoietic stem cells. EMBO J. *25*, 3515–3523.

Yan, Y., Frisén, J., Lee, M.H., Massagué, J., and Barbacid, M. (1997). Ablation of the CDK inhibitor $p57^{Kip2}$ results in increased apoptosis and delayed differentiation during mouse development. Genes Dev. *11*, 973–983.

Yuan, Y.Z., Shen, H.M., Franklin, D.S., Scadden, D.T., and Cheng, T. (2004). In vivo self-renewing divisions of haematopoietic stem cells are increased in the absence of the early G1-phase inhibitor, $p18^{INK4C}$. Nat. Cell Biol. *6*, 436–442.

Zhang, P., Liégeois, N.J., Wong, C., Finegold, M., Hou, H., Thompson, J.C., Silverman, A., Harper, J.W., DePinho, R.A., and Elledge, S.J. (1997). Altered cell differentiation and proliferation in mice lacking $p57^{KIP2}$ indicates a role in Beckwith-Wiedemann syndrome. Nature *387*, 151–158.

Zou, P., Arai, F., Yoshihara, H., Tai, I., Hosokawa, K., Matsumoto, Y., Shinmyozu, K., Tsukahara, F., Maru, Y., Nakayama, K., et al. (2011). $p57^{Kip2}$ and $p57^{Kip1}$ cooperate to maintain hematopoietic stem cell quiescence through interactions with Hsc70. Cell Stem Cell *9*, this issue, 247–261.

Research article

Fbxw7 regulates lipid metabolism and cell fate decisions in the mouse liver

Ichiro Onoyama,[1,2] Atsushi Suzuki,[3,4] Akinobu Matsumoto,[1,2] Kengo Tomita,[5] Hideki Katagiri,[6] Yuichi Oike,[4,7] Keiko Nakayama,[2,8] and Keiichi I. Nakayama[1,2]

[1]Department of Molecular and Cellular Biology, Medical Institute of Bioregulation, Kyushu University, Higashi-ku, Fukuoka, Fukuoka, Japan. [2]CREST, Japan Science and Technology Agency, Kawaguchi, Saitama, Japan. [3]Division of Organogenesis and Regeneration, Medical Institute of Bioregulation, Kyushu University, Higashi-ku, Fukuoka, Fukuoka, Japan. [4]PRESTO, Japan Science and Technology Agency, Kawaguchi, Saitama, Japan. [5]Division of Gastroenterology and Hepatology, Department of Internal Medicine, National Defense Medical College, Tokorozawa, Saitama, Japan. [6]Division of Advanced Therapeutics for Metabolic Diseases, Center for Translational and Advanced Animal Research, Tohoku University Graduate School of Medicine, Sendai, Japan. [7]Department of Molecular Genetics, Graduate School of Medical Sciences, Kumamoto University, Kumamoto, Japan. [8]Division of Developmental Genetics, Center for Translational and Advanced Animal Research, Tohoku University Graduate School of Medicine, Sendai, Japan.

E3 ubiquitin ligase complexes of the SCF type consist of ring-box 1 (Rbx1), cullin 1 (Cul1), S-phase kinase-associated protein 1 (Skp1), and a member of the F-box family of proteins. The identity of the F-box protein determines the substrate specificity of the complex. The F-box family member F-box– and WD repeat domain–containing 7 (Fbxw7; also known as Fbw7, SEL-10, hCdc4, and hAgo) targets for degradation proteins with wide-ranging functions, and uncovering its in vivo role has been difficult, because *Fbxw7*$^{-/-}$ embryos die in utero. Using two different Cre-loxP systems (*Mx1*-Cre and *Alb*-Cre), we generated mice with liver-specific null mutations of *Fbxw7*. Hepatic ablation of *Fbxw7* resulted in hepatomegaly and steatohepatitis, with massive deposition of triglyceride, a phenotype similar to that observed in humans with nonalcoholic steatohepatitis. Both cell proliferation and the abundance of Fbxw7 substrates were increased in the Fbxw7-deficient liver. Long-term Fbxw7 deficiency resulted in marked proliferation of the biliary system and the development of hamartomas. Fbxw7 deficiency also skewed the differentiation of liver stem cells toward the cholangiocyte lineage rather than the hepatocyte lineage in vitro. This bias was corrected by additional loss of the Notch cofactor RBP-J, suggesting that Notch accumulation triggered the abnormal proliferation of the biliary system. Together, our results suggest that Fbxw7 plays key roles, regulating lipogenesis and cell proliferation and differentiation in the liver.

Introduction

The abundance of cellular proteins is regulated in a coordinated manner at the levels of their synthesis and degradation. In particular, intracellular proteolysis is thought to be subject to highly specific regulation. The ubiquitin-proteasome system is responsible for such specific degradation of proteins, with ubiquitylation playing the regulatory role in this process. Ubiquitylation of target proteins is mediated by the sequential action of 3 enzymes: a ubiquitin-activating enzyme (E1), a ubiquitin-conjugating enzyme (E2), and a ubiquitin ligase (E3). The ubiquitylated substrates are then selectively recognized and degraded by the 26S proteasome (1). Uncontrolled proteolysis is implicated in dysregulation of cell proliferation and aberrant cell differentiation and is thought to underlie many human malignancies (2).

F-box proteins determine the substrate specificity of the SCF-type E3 complex, which consists of the RING-finger protein ring-box 1 (Rbx1; also known as Roc1 and Hrt1), the scaffold protein cullin 1 (Cul1), and the adaptor protein S-phase kinase-associated protein 1 (Skp1) in addition to an F-box protein (2–4). F-box– and WD repeat domain–containing 7 (Fbxw7; also known as Fbw7, SEL-10, hCdc4, and hAgo) is a member of the F-box protein family that was initially identified as a negative regulator of LIN-12–mediated (Notch-mediated) signaling in *Caenorhabditis elegans* by genetic analysis (5, 6). Fbxw7 also interacts with Notch family proteins and promotes their ubiquitin-dependent turnover in mammalian cells (5, 7, 8). Furthermore, it targets for degradation various mammalian proteins that control cell cycle progression (2, 4), including cyclin E (9–11), c-Myc (12, 13), and c-Jun (14, 15), as well as other proteins that do not contribute directly to cell cycle control, such as SREBPs (16–18), mammalian target of rapamycin (mTOR) (19), and PPAR-γ coactivator-1α (PGC-1α) (20).

Given its ability to promote degradation of cyclin E, c-Myc, c-Jun, and Notch, all of which are products of proto-oncogenes, Fbxw7 was expected to function as an oncosuppressor protein. Indeed, mutations in the *Fbxw7* gene have been detected in many types of human malignancy, including cholangiocarcinoma and T cell acute lymphoblastic leukemia as well as pancreatic, gastric, colorectal, prostate, and endometrial cancer (21–31). The study of Fbxw7 is thus important not only from the point of view of basic biology but also from the medical standpoint.

To analyze the functions of Fbxw7 in vivo, we and others have generated Fbxw7-deficient mice. However, *Fbxw7*$^{-/-}$ embryos were found to die in utero at E10.5, manifesting marked abnormalities in vascular development as a result of dysregulation of Notch signaling (32, 33). To avoid this early embryonic mortality, we have established mice in which *Fbxw7* is conditionally disrupted in T cells (34) or in hematopoietic stem cells (35), and we have also examined the effects of *Fbxw7* ablation in mouse embryonic fibroblasts (36). The loss of Fbxw7 in immature T cells results in the failure of these cells to exit the cell cycle, leading to thymic hyperplasia and the subsequent development of lymphoma. Among known targets of Fbxw7, only c-Myc and Notch accumulated in the Fbxw7-deficient thymocytes, and c-Myc accumulation was found

Conflict of interest: The authors have declared that no conflict of interest exists.

Citation for this article: *J Clin Invest.* 2010;121(1):342–354. doi:10.1172/JCI40725.

to be primarily responsible for the hyperproliferation phenotype. In contrast to that in immature T cells, the accumulation of c-Myc apparent in Fbxw7-null mature T cells induced expression of p53, which in turn led to cell cycle arrest and apoptosis. Furthermore, we found that Fbxw7 contributes to the long-term maintenance of hematopoietic stem cells. Most of the phenotypes of Fbxw7 deficiency in these conditional mouse mutants are related to cell proliferation or death and appear to be attributable to deregulation of c-Myc and Notch. Although Fbxw7 targets many substrates that do not participate directly in cell cycle control for degradation, the physiological roles of Fbxw7-mediated degradation of such targets have been largely unclear.

We have now examined the consequences of Fbxw7 deficiency in the liver. Unexpectedly, the major phenotypes associated with such deficiency were abnormalities in lipid metabolism and cell differentiation, which differ markedly from those in hematopoietic cell lineages and fibroblasts, in which Fbxw7 contributes primarily to the control of cell proliferation and apoptosis. We thus propose that Fbxw7 targets different groups of proteins for ubiquitin-dependent degradation and thereby contributes to distinct biological functions in a tissue-specific manner.

Results

Conditional inactivation of Fbxw7 in the liver by 2 Cre-loxP systems. We generated mice harboring floxed *Fbxw7* alleles (referred to herein as *Fbxw7*$^{F/F}$ mice) in which exon 5 (which encodes the F-box domain) is flanked by loxP sites (34). To ablate *Fbxw7* in the liver, we crossed these *Fbxw7*$^{F/F}$ mice with mice harboring a Cre transgene under the control of the promoter for the myxovirus resistance 1 (*Mx1*) or albumin (*Alb*) genes (*Mx1*-Cre or *Alb*-Cre mice). We confirmed that almost all floxed alleles were inactivated by Cre recombinase in the livers of *Alb*-Cre/*Fbxw7*$^{F/F}$ mice as well as in those of *Mx1*-Cre/*Fbxw7*$^{F/F}$ mice at 3 weeks after the last of 3 i.p. injections of poly(I)-poly(C) (pIpC) to activate the *Mx1* gene promoter (Figure 1A). For subsequent experiments, we examined the effects of short- or long-term Fbxw7 deficiency in *Mx1*-Cre/*Fbxw7*$^{F/F}$ mice and those of long-term a priori deficiency in *Alb*-Cre/*Fbxw7*$^{F/F}$ mice.

Massive lipid deposition and nonalcoholic steatohepatitis–like lesions in the Fbxw7-deficient liver. *Mx1*-Cre/*Fbxw7*$^{F/F}$ mice at 8 weeks of age were subjected to i.p. injection of pIpC every other day for 3 days to activate the *Mx1* gene promoter. At 3 weeks after the last injection of pIpC, the livers of these mice were enlarged and lighter in color compared with those of control animals (Figure 1B). The liver-to-body weight ratio of these *Mx1*-Cre/*Fbxw7*$^{F/F}$ mice was increased by approximately 30% relative to that of control mice (Figure 1C). Histological examination revealed that the nuclei of cells in the enlarged liver remained centrally located, whereas the corresponding cytoplasm was only weakly eosinophilic and contained numerous microvesicular vacuoles (Figure 1, D and E). Staining with Oil red O (Figure 1, F–I) also revealed massive lipid deposition, predominantly in the area around central veins (Figure 1G). Similar lipid deposition was also observed in the livers of *Alb*-Cre/*Fbxw7*$^{F/F}$ mice at as early as 12 weeks of age (Figure 1, J and K). The mechanism underlying such an uneven localization of lipid deposition is unclear and awaits further investigation.

Lobular infiltration of inflammatory cells such as lymphocytes and neutrophils (Figure 1, L and M; arrowhead), as well as the presence of many ballooned hepatocytes (occasionally containing Mallory body–like eosinophilic inclusions) (Figure 1, N and O; arrow), were observed in the livers of older mutant mice at approximately 50 weeks of age. Sinusoidal fibrogenic changes in the liver as revealed by Masson's trichrome staining were also evident (Figure 1, P and Q), and serum levels of aspartate aminotransferase (AST) and alanine aminotransferase (ALT) were significantly increased (Figure 1R) in *Alb*-Cre/*Fbxw7*$^{F/F}$ mice at 50 weeks of age. The serum level of bilirubin tended to be higher in the mutant animals than in age-matched controls, suggestive of the destruction of liver tissue in the mutant mice, although this difference was not statistically significant (Supplemental Figure 1; supplemental material available online with this article; doi:10.1172/JCI40725DS1). The onset of inflammatory changes occurred later than that of steatosis, but feeding *Mx1*-Cre/*Fbxw7*$^{F/F}$ mice a methionine- and choline-deficient (MCD) diet resulted in acceleration of inflammation (Figure 2A). The extents of steatosis and hepatitis were less pronounced in *Alb*-Cre/*Fbxw7*$^{F/F}$ mice than in *Mx1*-Cre/*Fbxw7*$^{F/F}$ mice subjected to acute ablation of Fbxw7, probably as a result of compensatory mechanisms operative during development in the former animals. However, massive steatosis and inflammation were also apparent in *Alb*-Cre/*Fbxw7*$^{F/F}$ mice fed the MCD diet, whereas control animals did not show such marked changes (Figure 2B). These results suggested that *Alb*-Cre/*Fbxw7*$^{F/F}$ mice are also more sensitive to steatohepatitis than are controls. The histological findings in both types of Fbxw7-deficient mice are highly similar to those associated with nonalcoholic steatohepatitis (NASH) in humans (37).

Expression of adipogenic and lipogenic genes in the Fbxw7-deficient liver. We next determined lipid concentrations in liver extracts. Triglyceride levels were significantly increased in the livers of *Mx1*-Cre/*Fbxw7*$^{F/F}$ mice compared with those in control animals at 3 weeks after the final pIpC injection, whereas the concentration of total cholesterol was not affected in the mutant livers (Figure 3A). Given that triglyceride synthesis is regulated predominantly by transcriptional activators, such as SREBPs, carbohydrate response element–binding protein (ChREBP), and PPAR-γ, we examined the expression of these proteins and their downstream targets in the liver. Immunoblot analysis revealed that the abundance of nuclear SREBP1, which is the major SREBP in the liver and a target of Fbxw7-mediated proteolysis (16, 17), was increased both in pIpC-injected *Mx1*-Cre/*Fbxw7*$^{F/F}$ mice and in *Alb*-Cre/*Fbxw7*$^{F/F}$ mice (Figure 3B and Supplemental Figure 2). The intensity of the more slowly migrating band, likely corresponding to the phosphorylated form of SREBP1, was especially increased, consistent with the previous observation that the phosphorylated forms of SREBPs are targeted by Fbxw7 (16–18), as is generally the case for Fbxw7 substrates (11, 34). In contrast, the amounts of ChREBP and PPAR-γ were decreased in the mutant mice compared with those in control animals, suggestive of the operation of a negative feedback loop triggered by triglyceride accumulation. Consistent with this notion, the abundance of *Pparg* mRNA in the liver was increased in SREBP cleavage–activating protein–deficient mice, in which the SREBP pathway is inactivated (38). The levels of PGC-1α and mTOR (total or phosphorylated forms) were unaffected by hepatic deletion of *Fbxw7*.

RT and real-time PCR analysis revealed that the abundance of mRNAs for the adipogenic and lipogenic transcriptional activators *SREBP1c*, *ChREBP*, and *Pparg* was decreased in the Fbxw7-deficient liver (Figure 3C), suggesting that the transcription of these genes is suppressed by a negative feedback loop triggered by the high level of triglyceride. At the protein level, the precursor form of SREBP1 was reduced, probably as a result of the decrease in the abundance of its mRNA, whereas the mature cleaved form was increased (Supplemental Figure 3). Among the downstream targets of SREBPs,

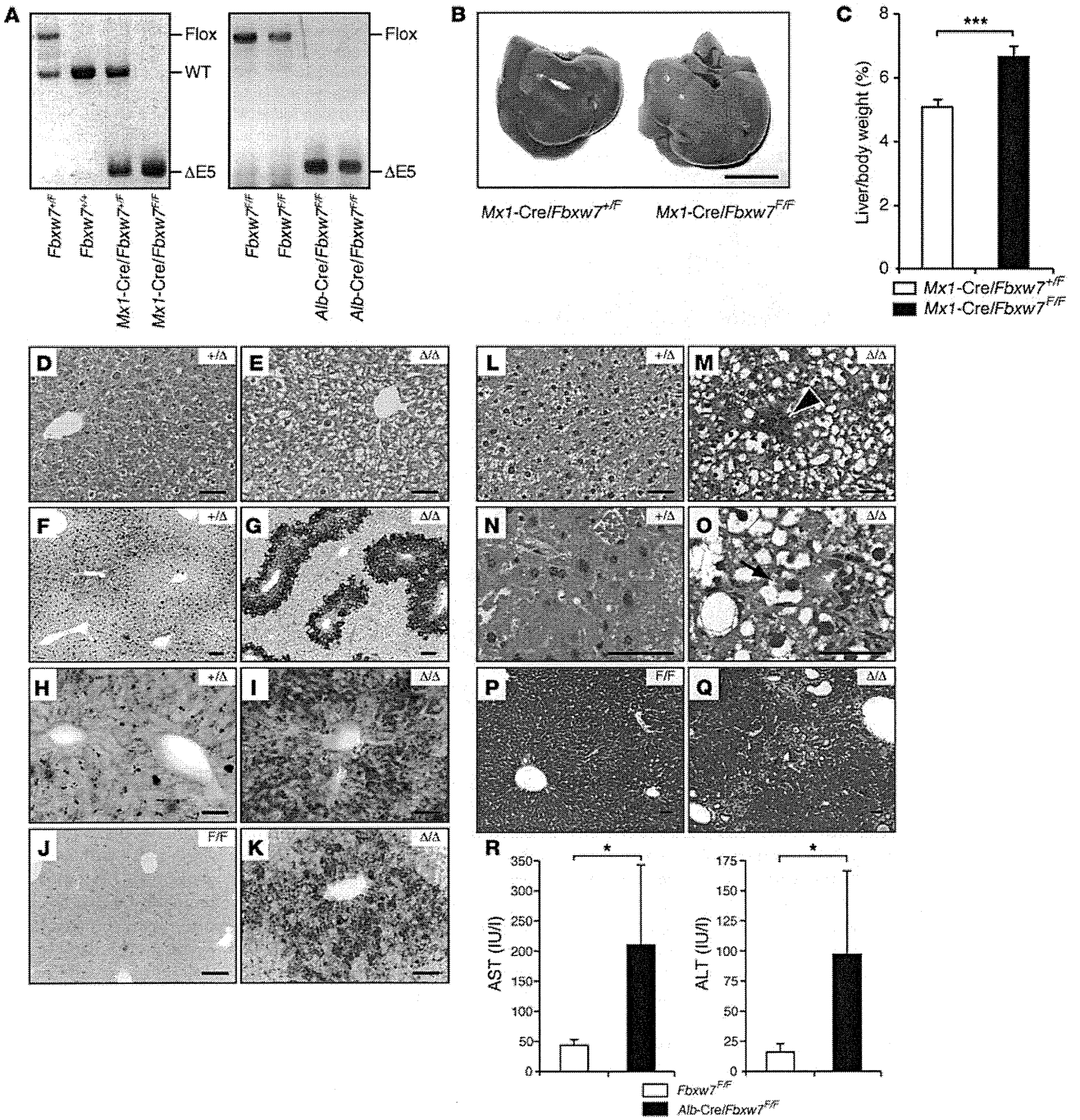

Figure 1

Development of NASH-like liver disease as a result of Fbxw7 deletion. (**A**) Genomic PCR analysis from the mouse liver of the indicated genotypes. The positions of amplified fragments corresponding to WT, floxed, and exon 5–deleted (ΔE5) alleles are indicated. (**B**) Gross appearance of the livers of indicated genotypes treated as in **A**. Scale bar: 10 mm. (**C**) Liver/body weight ratio of mice treated as in **A**. Data are mean ± SD from 5 animals of each genotype. ***$P < 0.005$. (**D** and **E**) H&E staining of liver sections from *Mx1*-Cre/*Fbxw7*$^{+/F}$ (+/Δ) and *Mx1*-Cre/*Fbxw7*$^{F/F}$ (Δ/Δ) mice, respectively, treated as in **A**. (**F** and **G**) Oil red O staining of liver sections treated as in **A**. (**H** and **I**) Higher-magnification views of images in **F** and **G**, respectively. (**J** and **K**) Oil red O staining of liver sections from *Fbxw7*$^{F/F}$ (F/F) and *Alb*-Cre/*Fbxw7*$^{F/F}$ (Δ/Δ) mice, respectively, at 12 weeks of age. (**L–O**) H&E staining of liver sections from *Mx1*-Cre/*Fbxw7*$^{+/F}$ (+/Δ) (**L** and **N**) and *Mx1*-Cre/*Fbxw7*$^{F/F}$ (Δ/Δ) (**M** and **O**) mice at 50 weeks after the final injection of pIpC. Lobular infiltration of inflammatory cells is indicated by the arrowhead, and Mallory body–like eosinophilic inclusion is indicated by the arrow. (**P** and **Q**) Masson's trichrome staining of liver sections from *Fbxw7*$^{F/F}$ (F/F) and *Alb*-Cre/*Fbxw7*$^{F/F}$ (Δ/Δ) mice, respectively, at 50 weeks of age. Scale bar: 50 μm (**D**, **E**, **H**, **I**, and **L–O**); 100 μm (**F**, **G**, **J**, **K**, **P**, and **Q**). (**R**) Serum AST and ALT activities in *Fbxw7*$^{F/F}$ ($n = 6$) and *Alb*-Cre/*Fbxw7*$^{F/F}$ ($n = 10$) mice at 50 weeks of age. Data are mean ± SD. *$P < 0.05$.

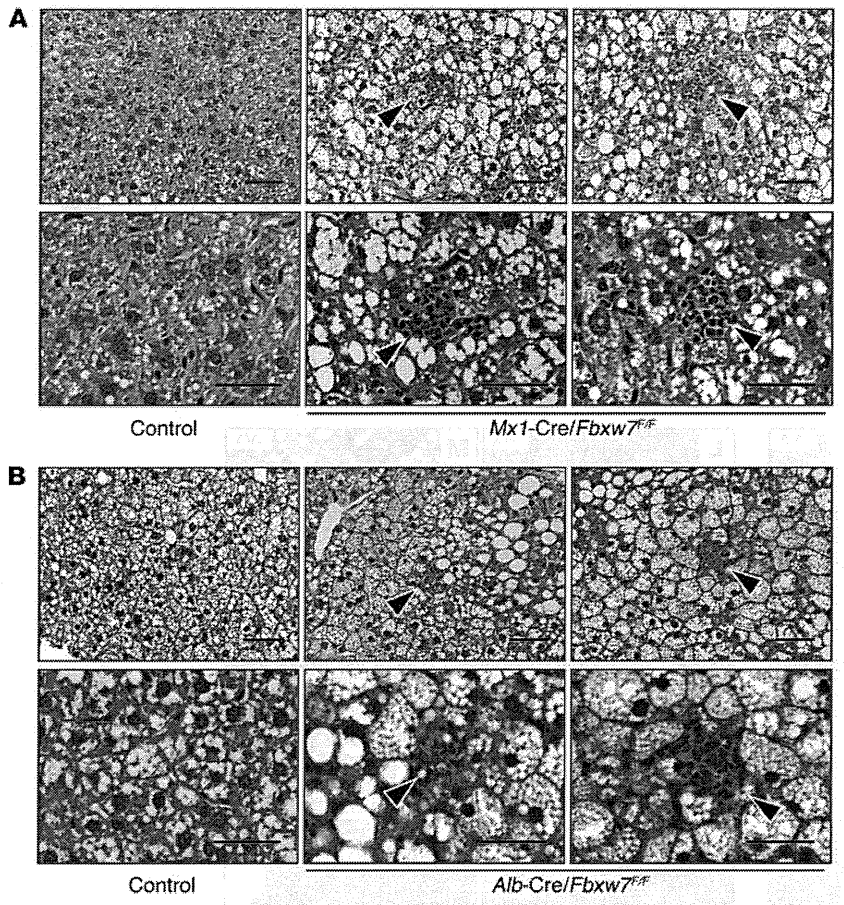

Figure 2
Increased susceptibility to a NASH-like condition conferred by Fbxw7 ablation in the liver. (**A**) *Mx1*-Cre/*Fbxw7*$^{+/F}$ (control) and *Mx1*-Cre/*Fbxw7*$^{F/F}$ mice were injected with pIpC at 8 weeks of age and then fed an MCD diet for 2 weeks. Liver sections were then subjected to H&E staining. Lower- and higher-magnification views are shown (top and bottom panels, respectively). In addition to fatty degeneration, many foci of lobular infiltration of inflammatory cells (arrowheads) were apparent in the livers of *Mx1*-Cre/*Fbxw7*$^{F/F}$ mice. Scale bar: 50 μm. (**B**) *Alb*-Cre/*Fbxw7*$^{+/F}$ (control) and *Alb*-Cre/*Fbxw7*$^{F/F}$ mice at 12 weeks of age were fed an MCD diet for 4 weeks and then analyzed as in **A**. Lower- and higher-magnification views are shown (top and bottom panels, respectively). Control mice developed a small extent of fatty degeneration, whereas *Alb*-Cre/*Fbxw7*$^{F/F}$ mice showed massive accumulation of lipid droplets and many foci of lobular infiltration of inflammatory cells (arrowheads) similar to those apparent in *Mx1*-Cre/*Fbxw7*$^{F/F}$ mice. Scale bar: 50 μm.

the amounts of mRNAs for fatty acid synthase (*Fas*) and stearoyl-CoA desaturase-1 (*Scd1*) were increased, whereas those for the LDL receptor (*Ldlr*) and HMG-CoA synthase (*Hmgcs1*) were decreased, in the mutant liver (Figure 3C). Immunostaining also showed that SREBP1 accumulated in the region around the central veins (Figure 3D), corresponding to the area of lipid deposition, even though deletion of *Fbxw7* appears to occur throughout almost the entire liver. The expression of SCD-1 was also increased in the region around the central veins in which SREBP1 was upregulated (Figure 3E). Collectively, these results suggested that the accumulation of SREBP proteins as a result of Fbxw7 ablation results in triglyceride deposition in the liver, which in turn affects the expression of other adipogenic and lipogenic genes as well as their downstream targets via a negative feedback loop.

Increased proliferation of Fbxw7-deficient hepatocytes. We compared the abundance of cyclin E and c-Myc between the livers of *Mx1*-Cre/*Fbxw7*$^{+/F}$ and *Mx1*-Cre/*Fbxw7*$^{F/F}$ mice at 3 or 50 weeks after the final pIpC injection, beginning at 8 weeks of age. Immunoblot analysis revealed that the amount of cyclin E in the livers of *Mx1*-Cre/*Fbxw7*$^{F/F}$ mice was increased compared with that in *Mx1*-Cre/*Fbxw7*$^{+/F}$ mice at 3 weeks after pIpC injection but not at 50 weeks (Figure 4A). The abundance of c-Myc was not affected by the loss of Fbxw7 in the liver, at either 3 or 50 weeks after injection. To measure the rate of hepatocyte proliferation, we subjected *Mx1*-Cre/*Fbxw7*$^{+/F}$ and *Mx1*-Cre/*Fbxw7*$^{F/F}$ mice to i.p. injection with BrdU for 3 consecutive days, beginning at 3 or 50 weeks after the final pIpC injection. Immunostaining of the liver with antibodies to BrdU at 1 day after the last BrdU injection revealed that the rate of BrdU incorporation was markedly increased in Fbxw7-deficient liver cells compared with that in control cells (Figure 4B). Most of the BrdU-positive cells were also reactive with antibodies to albumin but not with those to cytokeratin 19 (CK19) at 3 weeks after pIpC injection (Figure 4C), suggesting that the proliferating cells are predominantly hepatocytes. In contrast, at 50 weeks after pIpC injection, both hepatocytes and cholangiocytes in *Mx1*-Cre/*Fbxw7*$^{F/F}$ mice incorporated BrdU to a greater extent than did those in control mice. The TUNEL assay revealed that the frequency of apoptosis was also increased in the Fbxw7-deficient liver at 3 weeks after pIpC injection (Figure 4, D and E), suggesting that the loss of Fbxw7 transiently promotes cell cycle progression but eventually results in apoptosis in the liver, as it does in T lymphocytes (34).

Development of hamartomas with hyperproliferation of the biliary system in the Fbxw7-deficient liver. We next examined in more detail the long-term effects of Fbxw7 loss in the liver. Macroscopic examination of *Mx1*-Cre/*Fbxw7*$^{F/F}$ mice at 50 weeks after pIpC injection at 8 weeks of age revealed that the mutant liver was enlarged and darker in color compared with the control liver and possessed a rough surface as a result of the presence of several nodules (Figure 5A). We confirmed that the *Fbxw7* gene was deleted in such nodules (Figure 5B), which were grossly demarcated and readily excised from the liver. Histological examination revealed structural abnormalities characterized by marked dilation of intrahepatic bile ducts as well as apparent proliferation of the biliary system

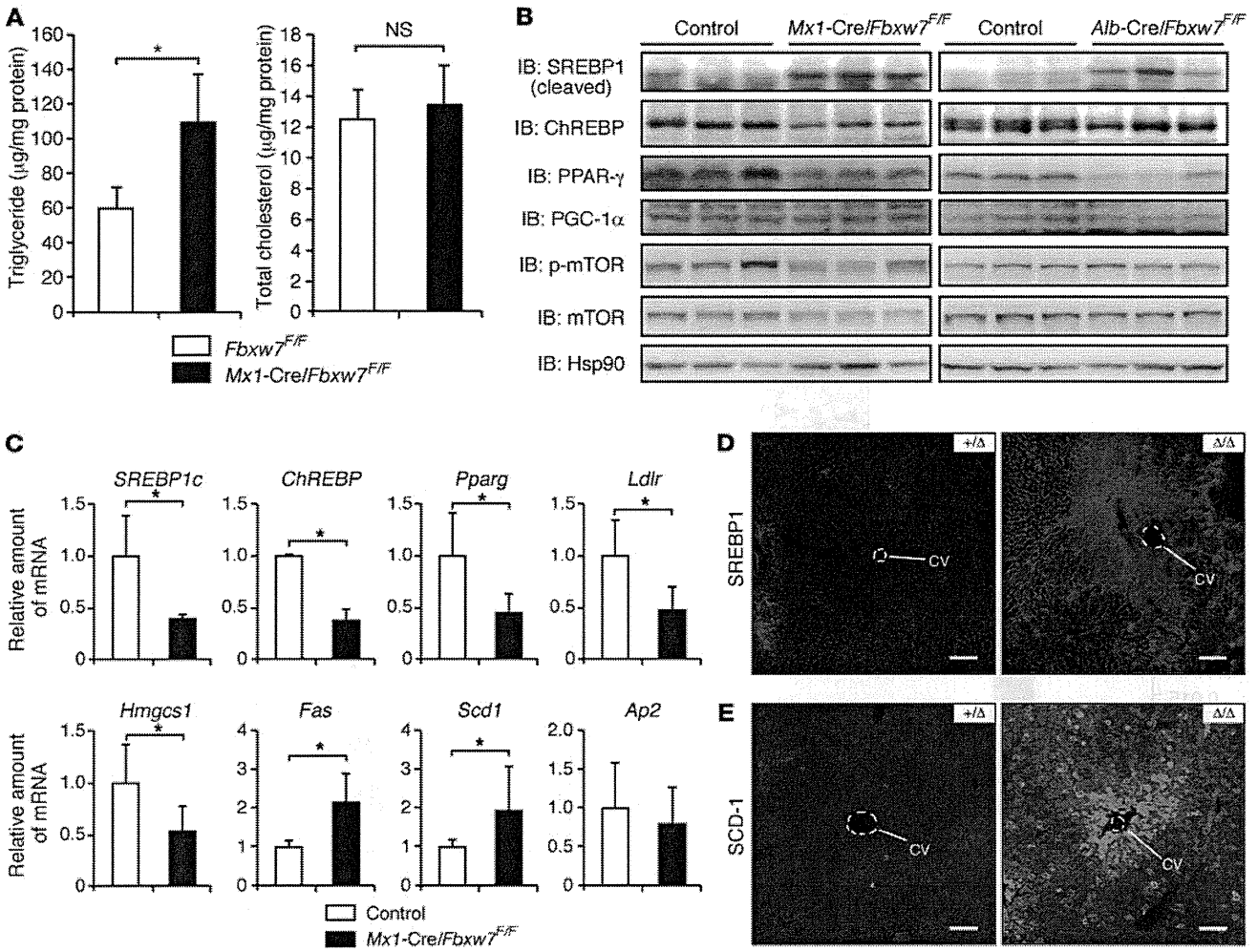

Figure 3

Deposition of triglyceride and accumulation of SREBP1 in the Fbxw7-deficient liver. (**A**) Triglyceride and total cholesterol concentrations in the livers of *Mx1*-Cre/*Fbxw7*$^{+/F}$ (control) and *Mx1*-Cre/*Fbxw7*$^{F/F}$ mice at 3 weeks after the final injection of pIpC, beginning at 8 weeks of age. Data are mean ± SD from 3 mice of each genotype. *$P < 0.05$. (**B**) Protein extracts of the livers of *Mx1*-Cre/*Fbxw7*$^{+/F}$ (control) and *Mx1*-Cre/*Fbxw7*$^{F/F}$ mice at 3 weeks after the final injection of pIpC, beginning at 8 weeks of age, were subjected to IB analysis with antibodies to the indicated proteins (left panel). Liver extracts of *Fbxw7*$^{F/F}$ (control) and *Alb*-Cre/*Fbxw7*$^{F/F}$ mice at 12 weeks of age were similarly analyzed (right panel). Three animals were examined for each genotype. Hsp90 was analyzed as a loading control. p-mTOR, phosphorylated mTOR. (**C**) RT and real-time PCR analysis of the indicated mRNAs in the livers of *Mx1*-Cre/*Fbxw7*$^{+/F}$ (control) and *Mx1*-Cre/*Fbxw7*$^{F/F}$ mice treated as in **A**. Normalized data are expressed relative to the corresponding value for control mice and are mean ± SD from 3 independent experiments. *$P < 0.05$. (**D** and **E**) Liver sections of *Mx1*-Cre/*Fbxw7*$^{+/F}$ (+/Δ) and *Mx1*-Cre/*Fbxw7*$^{F/F}$ (Δ/Δ) mice, treated as in **A**, were subjected to immunofluorescence staining with antibodies (**D**) to SREBP1 and (**E**) to SCD-1. CV, central vein. Scale bar: 100 μm.

(Figure 5, C–F); these abnormalities were pathologically diagnosed as hamartomas. Such lesions were also observed, albeit to a lesser extent, in *Alb*-Cre/*Fbxw7*$^{F/F}$ mice at as early as 12 weeks of age (Figure 5, G and H). Hamartomas, which are reactive with antibodies to CK19 (Figure 5, I and J), developed in all mutant mice of both genotypes examined ($n = 14$). These results suggested that the loss of Fbxw7 may promote proliferation of the biliary system and shift the development of hepatic stem cells toward the cholangiocyte lineage rather than the hepatocyte lineage.

We examined the abundance of mRNAs for *Alb* (Figure 5K) and *CK19* (Figure 5L) as markers of hepatocyte and cholangiocyte lineages, respectively. The amount of *CK19* mRNA in the liver was increased as early as 2 weeks after pIpC injection in *Mx1*-Cre/*Fbxw7*$^{F/F}$ mice and showed a more than 40-fold increase at 50 weeks after *Fbxw7* deletion. In contrast, the abundance of *Alb* mRNA in the mutant liver at 50 weeks after pIpC injection was decreased by 40% compared with that in control liver. These changes in differentiation markers were thus consistent with a marked proliferation of the biliary system in the Fbxw7-deficient liver.

Skewed hepatic differentiation induced by Notch1 accumulation in the Fbxw7-deficient liver. The hepatic cell fate decision is thought to be largely dependent on Notch signaling (39–44). We therefore examined the expression of Notch, a target of Fbxw7, in the Fbxw7-deficient liver. Although immunoblot analysis did not reveal an

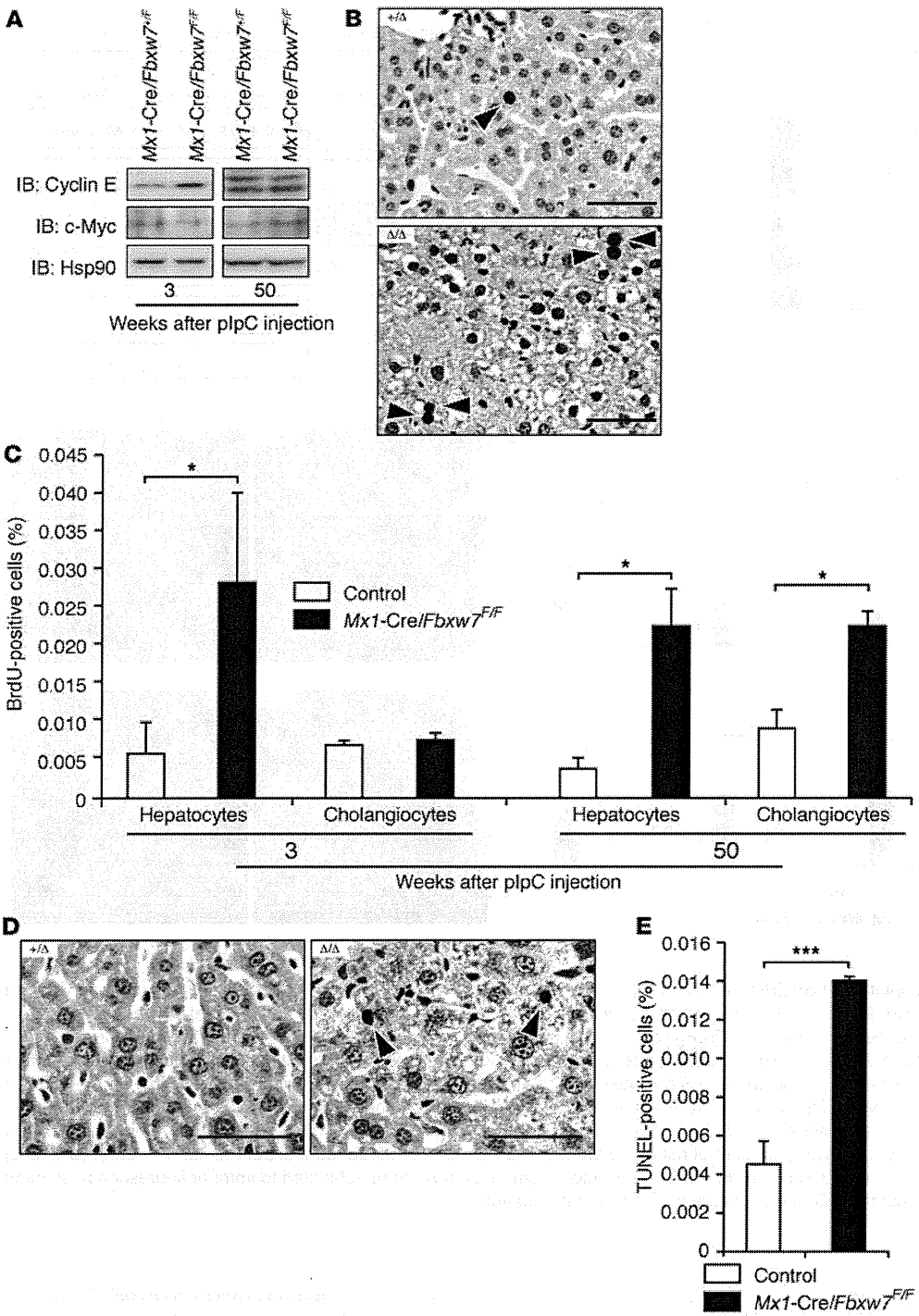

Figure 4
Increased proliferation and apoptosis of Fbxw7-deficient hepatocytes. (**A**) IB analysis of cyclin E, c-Myc, and Hsp90 (loading control) in liver extracts from *Mx1*-Cre/*Fbxw7*$^{+/F}$ and *Mx1*-Cre/*Fbxw7*$^{F/F}$ mice at 3 or 50 weeks after *Fbxw7* deletion by pIpC injection, beginning at 8 weeks of age. (**B**) Representative immunostaining for BrdU in liver sections from *Mx1*-Cre/*Fbxw7*$^{+/F}$ (+/Δ) and *Mx1*-Cre/*Fbxw7*$^{F/F}$ (Δ/Δ) mice injected with BrdU on 3 consecutive days, beginning 3 weeks after the final pIpC injection as in **A**. Arrowheads indicate BrdU-positive nuclei. Scale bar: 50 μm. (**C**) The proportion of BrdU-positive hepatocytes or cholangiocytes was determined from immunostaining for BrdU in combination with that for albumin or CK19 in the livers of *Mx1*-Cre/*Fbxw7*$^{+/F}$ (control) or *Mx1*-Cre/*Fbxw7*$^{F/F}$ mice at 3 or 50 weeks after deletion of *Fbxw7* as in **A**. Data are mean ± SD from 10 fields from 3 mice of each genotype. *$P < 0.05$. (**D**) Representative TUNEL staining for liver sections of *Mx1*-Cre/*Fbxw7*$^{+/F}$ (+/Δ) and *Mx1*-Cre/*Fbxw7*$^{F/F}$ (Δ/Δ) mice 3 weeks after the final pIpC injection as in **A**. Arrowheads indicate TUNEL-positive cells. Scale bar: 50 μm. (**E**) The proportion of TUNEL-positive liver cells was determined from images similar to those in **D**. Data are mean ± SD from 3 animals of each genotype. ***$P < 0.005$.

increase in the abundance of any of the isoforms of Notch in the liver of *Mx1*-Cre/*Fbxw7*$^{F/F}$ mice at either 3 or 50 weeks after *Fbxw7* deletion (data not shown), confocal microscopic analysis revealed that the intracellular domain of Notch1 was highly concentrated in both the cytoplasm and the nucleus of Fbxw7-deficient liver at 3 weeks after pIpC injection (Figure 6A). Consistent with the observed upregulation of Notch1, the abundance of Notch1 target genes, including those for Hes1 and Hey1, was simultaneously increased in the livers of *Mx1*-Cre/*Fbxw7*$^{F/F}$ mice (Figure 6B and Supplemental Figure 5A, respectively). At 15 weeks after pIpC injection, Notch1 accumulated in the hepatocyte-like cells residing around the portal area, and these cells were reactive to antibodies to CK7 (Figure 6C), another marker of cholangiocytes, suggesting that such cells might be in the process of transdifferentiation to the cholangiocytes by Notch activation. At 50 weeks after pIpC injection, Notch1 was observed in the form of aggregates in the

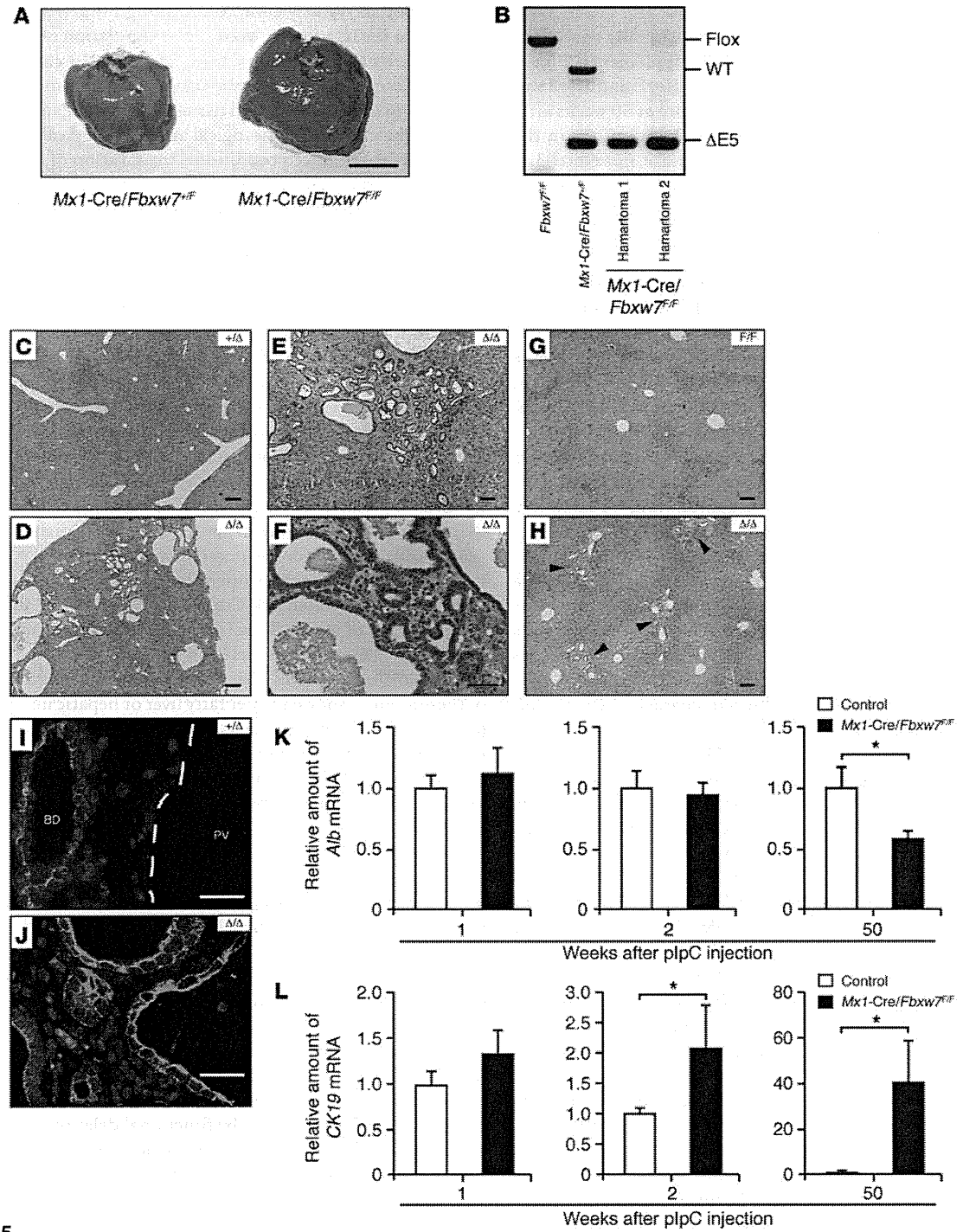

Figure 5

Hamartoma development as a result of long-term ablation of Fbxw7 in the liver. (**A**) Gross appearance of the livers of *Mx1*-Cre/*Fbxw7*$^{+/F}$ and *Mx1*-Cre/*Fbxw7*$^{F/F}$ mice at 50 weeks after the final injection of pIpC, beginning at 8 weeks of age. Scale bar: 10 mm. (**B**) PCR analysis of genomic DNA from the dilated bile ducts excised from hamartomas in the livers of 2 *Mx1*-Cre/*Fbxw7*$^{F/F}$ mice. Genomic DNA from control mice was also analyzed. (**C–F**) H&E staining of liver sections from a *Mx1*-Cre/*Fbxw7*$^{+/F}$ (+/Δ) mouse (**C**) and from a *Mx1*-Cre/*Fbxw7*$^{F/F}$ (Δ/Δ) mouse (**D–F**) that developed hamartoma after *Fbxw7* deletion as in **A**. (**G** and **H**) H&E staining of liver sections from *Fbxw7*$^{F/F}$ (F/F) and *Alb*-Cre/*Fbxw7*$^{F/F}$ (Δ/Δ) mice, respectively, at 12 weeks of age. Arrowheads indicate malformation of the ductal plate. Scale bar: 50 μm (**F**); 100 μm (**E**, **G**, and **H**); 200 μm (**C** and **D**). (**I** and **J**) Immunofluorescence staining for CK19 in the livers of *Mx1*-Cre/*Fbxw7*$^{+/F}$ (+/Δ) and *Mx1*-Cre/*Fbxw7*$^{F/F}$ (Δ/Δ) mice at 50 weeks after the final injection of pIpC, beginning at 8 weeks of age. The dashed line indicates the outer boundary of portal vein. PV, portal vein; BD, bile duct. Scale bar: 25 μm. (**K** and **L**) RT and real-time PCR analysis of *Alb* and *CK19* mRNAs, respectively, in the livers of *Mx1*-Cre/*Fbxw7*$^{+/F}$ (control) and *Mx1*-Cre/*Fbxw7*$^{F/F}$ mice at 1, 2, or 50 weeks after deletion of *Fbxw7* as in **A**. Normalized data are expressed relative to the corresponding value for control mice. Data are mean ± SD from 3 independent experiments. *$P < 0.05$.

cytoplasm or the nucleus (Supplemental Figure 4A). The increase in Hes1 or Hey1 was not detected by immunostaining analysis at this period (Supplemental Figure 4B and Supplemental Figure 5B), but the abundance of mRNAs for *Hes1*, *Hey1*, and *Hey2* was increased in the livers of *Mx1*-Cre/*Fbxw7*$^{F/F}$ mice at 50 weeks after pIpC injection (Figure 6D). Neither Notch2, mutations in the gene in which mutations result in Alagille disease, nor Notch3 or Notch4, the expression of both of which is increased in hepatocellular carcinoma, were detected by immunofluorescence analysis in the livers of either control or *Mx1*-Cre/*Fbxw7*$^{F/F}$ mice (data not shown). However, neither the expression of Notch ligands, such as Dll-1 and Jagged-1, nor that of the Notch cofactor RBP-J in the liver appeared to be affected by the loss of Fbxw7 (Supplemental Figure 6). We also examined the expression of TSC1 and TSC2, given that the loss of function of either TSC1 or TSC2 is known to result in the development of hamartoma in humans. However, no difference in expression of TSC1 or TSC2 was found between Fbxw7-deficient and control mice (Supplemental Figure 6).

To investigate whether the skewed developmental orientation toward the cholangiocyte lineage apparent in the Fbxw7-deficient liver is dependent on Notch1 accumulation, we examined the differentiation of hepatic stem cells in culture (45). A fraction containing hepatic stem cells was prepared from the livers of *Fbxw7*$^{+/F}$ and *Fbxw7*$^{F/F}$ embryos and was then infected with a retrovirus encoding Cre recombinase or with the empty virus alone to generate *Fbxw7*$^{+/F}$, *Fbxw7*$^{+/\Delta}$, *Fbxw7*$^{F/F}$, and *Fbxw7*$^{\Delta/\Delta}$ cells in the presence of HGF and EGF. Immunofluorescence analysis revealed that most of the *Fbxw7*$^{+/F}$, *Fbxw7*$^{+/\Delta}$, and *Fbxw7*$^{F/F}$ cells differentiated into the hepatocyte lineage, characterized by albumin expression, with only a small subset of cells differentiating into the cholangiocyte lineage (Figure 7A). In contrast, the percentage of *Fbxw7*$^{\Delta/\Delta}$ cells that differentiated into the cholangiocyte lineage, characterized by expression of CK7, was markedly increased compared with that for cells of the control genotypes. To confirm these results in a quantitative manner, we performed RT and real-time PCR analysis of *Alb* and *CK19* mRNAs. Consistent with the immunofluorescence data, the amount of *CK19* mRNA was significantly increased in *Fbxw7*$^{\Delta/\Delta}$ cells compared with that in *Fbxw7*$^{+/\Delta}$ cells, whereas the abundance of *Alb* mRNA did not differ between the 2 genotypes (Figure 7B).

Notch signaling is implicated in the differentiation of liver stem cells into the cholangiocyte lineage. Indeed, immunofluorescence analysis revealed that Notch1 accumulated in *Fbxw7*$^{\Delta/\Delta}$ cells to a greater extent than in *Fbxw7*$^{+/\Delta}$ cells (Supplemental Figure 7). We therefore examined whether additional ablation of the Notch cofactor RBP-J might correct the abnormal development of Fbxw7-deficient liver stem cells. We generated Fbxw7-deficient hepatic stem cells with additional deletion of either *Rbpj* or *Myc* genes and examined the level of *CK19* mRNA. The abundance of *CK19* mRNA was increased in *Fbxw7*$^{\Delta/\Delta}$*Myc*$^{\Delta/\Delta}$ cells but not in *Fbxw7*$^{\Delta/\Delta}$*Rbpj*$^{\Delta/\Delta}$ cells (Figure 7B). These results indicate that the skewed developmental orientation of hepatic stem cells to the cholangiocyte lineage is dependent on Notch1 accumulation induced by the loss of Fbxw7.

Discussion

Given that the substrates of Fbxw7 include key proteins that contribute to diverse biological processes, including the cell cycle, cell differentiation, and apoptosis, and that the binding of Fbxw7 to its substrates depends on their phosphorylation, the function of this protein is likely complex. Although much attention has focused on the relation between the accumulation of cyclin E due to loss of Fbxw7 function and tumorigenesis, Notch degradation by Fbxw7 is critical during embryogenesis, suggesting that Fbxw7 functions in development- and tissue-dependent manners. To provide insight into the physiological and pathological relevance of Fbxw7, we have induced conditional inactivation of *Fbxw7* in several mouse tissues. Our previous studies have shown that ablation of *Fbxw7* in hematopoietic cells or fibroblasts results in abnormalities that are mainly related to the cell cycle and apoptosis. We now show that liver-specific ablation of *Fbxw7* induced fatty liver and abnormal cell differentiation, likely as a result of the accumulation of SREBPs and Notch1, respectively, as well as promoted cell proliferation (Figure 8).

We generated 2 types of mice with liver-specific deficiency of Fbxw7 with the use of the *Mx1* or *Alb* gene promoters to drive Cre expression. The phenotypes of *Alb*-Cre/*Fbxw7*$^{F/F}$ mice are milder than those induced by acute ablation of Fbxw7 in *Mx1*-Cre/*Fbxw7*$^{F/F}$ mice, probably because of the operation of compensatory mechanisms during development in the former animals. In *Mx1*-Cre/*Fbxw7*$^{F/F}$ mice, it would be expected for *Fbxw7* to be deleted in cells and tissues other than the liver, such as hematopoietic cells. To exclude the possibility that ablation of Fbxw7 in hematopoietic cell lineages might be responsible for steatohepatitis, we have generated Lck-Cre/*Fbxw7*$^{F/F}$ and CD4-Cre/*Fbxw7*$^{F/F}$ mice (in both of which *Fbxw7* deletion occurs in T cells), CD19-Cre/*Fbxw7*$^{F/F}$ mice (*Fbxw7* deletion occurs in B cells), and LysM-Cre/*Fbxw7*$^{F/F}$ mice (*Fbxw7* deletion occurs in myeloid cells). None of these animals showed either fatty liver or hepatic inflammation (data not shown). Furthermore, *Alb*-Cre/*Fbxw7*$^{F/F}$ mice manifested pronounced hepatic infiltration of inflammatory cells when they were fed an MCD diet, confirming that the steatohepatitis induced by *Fbxw7* deletion is attributable to an effect that is intrinsic to the liver.

Nonalcoholic fatty liver disease (NAFLD) is a growing health concern, due to its rapidly increasing prevalence worldwide. NASH is a progressive form of NAFLD that has the potential to develop into hepatocellular carcinoma. We now show that mice with liver-specific ablation of Fbxw7 developed clinicopathologic features similar to those of NAFLD or NASH in humans, including triglyceride deposition around central veins, pericellular fibrosis, infiltration of inflammatory mononuclear cells, and the appearance of Mallory bodies in the liver as well as increases in the serum levels of ALT and AST. However, these animals were not found to develop hepatocellular carcinoma. Genetic mouse models for human NASH have been established by functional deletion of leptin (46) or its receptor (47), phosphatase and tensin homolog (PTEN) (48), NEMO (also known as IKK-γ) (49), interleukin-1 receptor α (50), galectin-3 (51), or retinoic acid receptor α (52). Mice transgenic for SREBP1c also manifest pronounced NASH (53). SREBP1c is degraded in an Fbxw7-dependent manner (16), and we have now shown that it accumulated in the Fbxw7-deficient liver. These findings thus suggest that an Fbxw7-SREBP1 axis plays a key physiological role in the regulation of lipid metabolism in the liver as well as a pathological role in the development of NASH.

Whereas steatosis develops in the acute phase of liver-specific Fbxw7 deficiency, hamartoma develops in the chronic phase. Fbxw7 targets mTOR for degradation (19). The TSC complex, consisting of TSC1 (hamartin) and TSC2 (tuberin), is the major negative regulator of mTOR, and its genetic loss results in mTOR